Article

Developmental Cell

Reprogramming Axial Level Identity to Rescue Neural-Crest-Related Congenital Heart Defects

Graphical Abstract

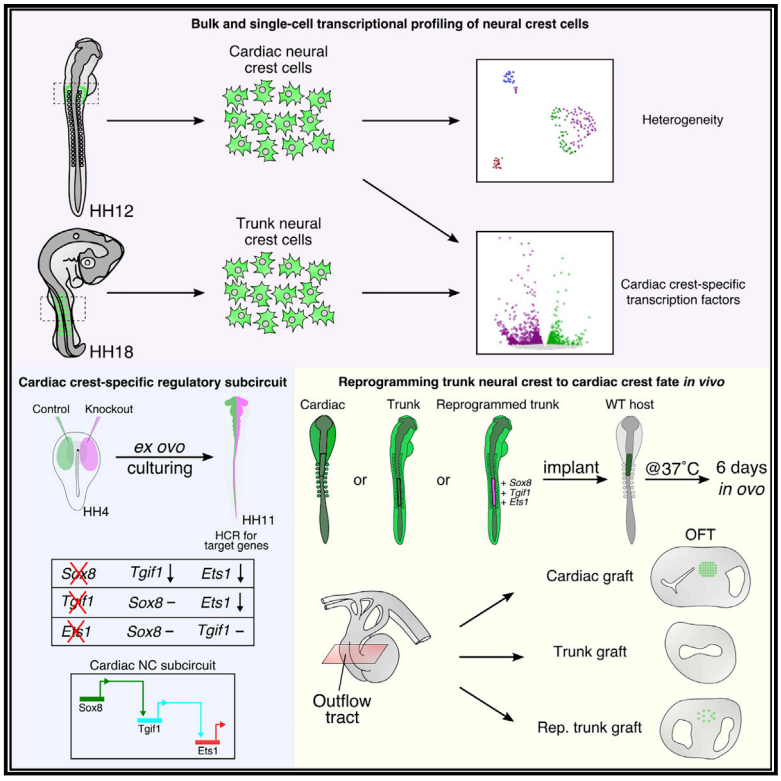

Highlights

- Ablations reveal laterality differences in neural crest contributions to the heart
- Transcriptional profiling reveals *Tgif1* as critical for outflow tract morphogenesis
- *Sox8, Tgif1*, and *Ets1* comprise a regulatory subcircuit for cardiac crest specification
- Expression of subcircuit genes in trunk reprograms them toward cardiac-crest-like fate

Authors

Shashank Gandhi, Max Ezin, Marianne E. Bronner

Correspondence

mbronner@caltech.edu

In Brief

Here, Gandhi et al. identify a molecular subcircuit comprised of transcription factors *Sox8, Tgif1*, and *Ets1* that confers cardiac neural crest cells with their unique ability to contribute to the heart. Moreover, expression of this subcircuit is sufficient to reprogram trunk neural crest cells to adopt a cardiac-crest-like identity.

Gandhi et al., 2020, Developmental Cell *53*, 300–315
May 4, 2020
https://doi.org/10.1016/j.devcel.2020.04.005

CellPress

CellPress

Developmental Cell

Article

Reprogramming Axial Level Identity to Rescue Neural-Crest-Related Congenital Heart Defects

Shashank Gandhi,[1] Max Ezin,[2] and Marianne E. Bronner[1,3,*]
[1]Division of Biology and Biological Engineering, California Institute of Technology, Pasadena, CA 91125, USA
[2]Department of Biology, Loyola Marymount University, Los Angeles, CA 90045, USA
[3]Lead Contact
*Correspondence: mbronner@caltech.edu
https://doi.org/10.1016/j.devcel.2020.04.005

SUMMARY

The cardiac neural crest arises in the hindbrain, then migrates to the heart and contributes to critical structures, including the outflow tract septum. Chick cardiac crest ablation results in failure of this septation, phenocopying the human heart defect persistent truncus arteriosus (PTA), which trunk neural crest fails to rescue. Here, we probe the molecular mechanisms underlying the cardiac crest's unique potential. Transcriptional profiling identified cardiac-crest-specific transcription factors, with single-cell RNA sequencing revealing surprising heterogeneity, including an ectomesenchymal subpopulation within the early migrating population. Loss-of-function analyses uncovered a transcriptional subcircuit, comprised of *Tgif1, Ets1*, and *Sox8*, critical for cardiac neural crest and heart development. Importantly, ectopic expression of this subcircuit was sufficient to imbue trunk crest with the ability to rescue PTA after cardiac crest ablation. Together, our results reveal a transcriptional program sufficient to confer cardiac potential onto trunk neural crest cells, thus implicating new genes in cardiovascular birth defects.

INTRODUCTION

The vertebrate heart arises from cells in the lateral plate mesoderm that converge at the embryonic midline and fuse into a heart tube. In amniotes, cells from the second heart field are added after the heart tube loops, causing remodeling of the tube to form four heart chambers—two atria and two ventricles. The looped heart connects to the forming lungs by means of the truncus arteriosus, which initially is a single vessel destined to form the outflow tract of the heart. Cardiac neural crest cells make a critical contribution to the heart by septating the truncus arteriosus into the pulmonary trunk, through which deoxygenated blood flows to the lungs, and the aortic trunk, through which oxygenated blood is pumped throughout the body. In fact, abnormal cardiac crest development results in some of the most common human congenital heart defects (Grossfeld et al., 2004; Loffredo, 2000; Neeb et al., 2013), including persistent truncus arteriosus (PTA), in which the aorticopulmonary septum fails to close, resulting in mixing of oxygenated and deoxygenated blood.

Premigratory cardiac neural crest cells initially reside within the developing caudal hindbrain, from which they migrate to the forming pharyngeal arches 3, 4, and 6 (Phillips et al., 1987). While some cells remain in the arches, contributing to the carotid and other arteries (Waldo and Kirby, 1993), others invade the heart to form the aorticopulmonary septum, cardiac cushions, part of the interventricular septum, and cardiac ganglia (Kirby and Stewart, 1983). A small number of neural crest cells also move through arches 1 and 2 to the right ventricle, where they adopt coronary smooth muscle fates (Arima et al., 2012).

Loss of genes that are important for cardiac neural crest development, such as *Pax3* or *Edn1* (endothelin-1), results in cardiac abnormalities (Franz, 1989; Kurihara et al., 1999). Moreover, surgical ablation of the cardiac crest in chick (Kirby and Waldo, 1990; Kirby et al., 1985) phenocopies human PTA (Besson et al., 1986; Kirby and Waldo, 1995; Nishibatake et al., 1987). Importantly, grafting cranial or trunk neural crest in place of ablated cardiac crest cannot rescue the deficit (Kirby, 1989), suggesting that inherent differences exist along the body axis in the neural crest's ability to form cardiovascular derivatives. However, the mechanisms underlying the cardiac crest's unique developmental potential remain unknown.

Here, we tackle the molecular and cellular basis of cardiac-crest-related birth defects by combining classical embryology with state-of-the-art genomics approaches. First, we reproduce and extend classical chick embryological experiments done over 30 years ago and report laterality differences in cardiovascular defects resulting from unilateral cardiac neural fold ablations. Second, we identify new genes enriched in the cardiac neural crest by bulk and single-cell RNA sequencing (scRNA-seq) and demonstrate that migrating cardiac crest cells represent a heterogeneous population. Third, we establish regulatory relationships of cardiac neural crest genes and explore their role in heart development. Accordingly, we find that one of these genes,

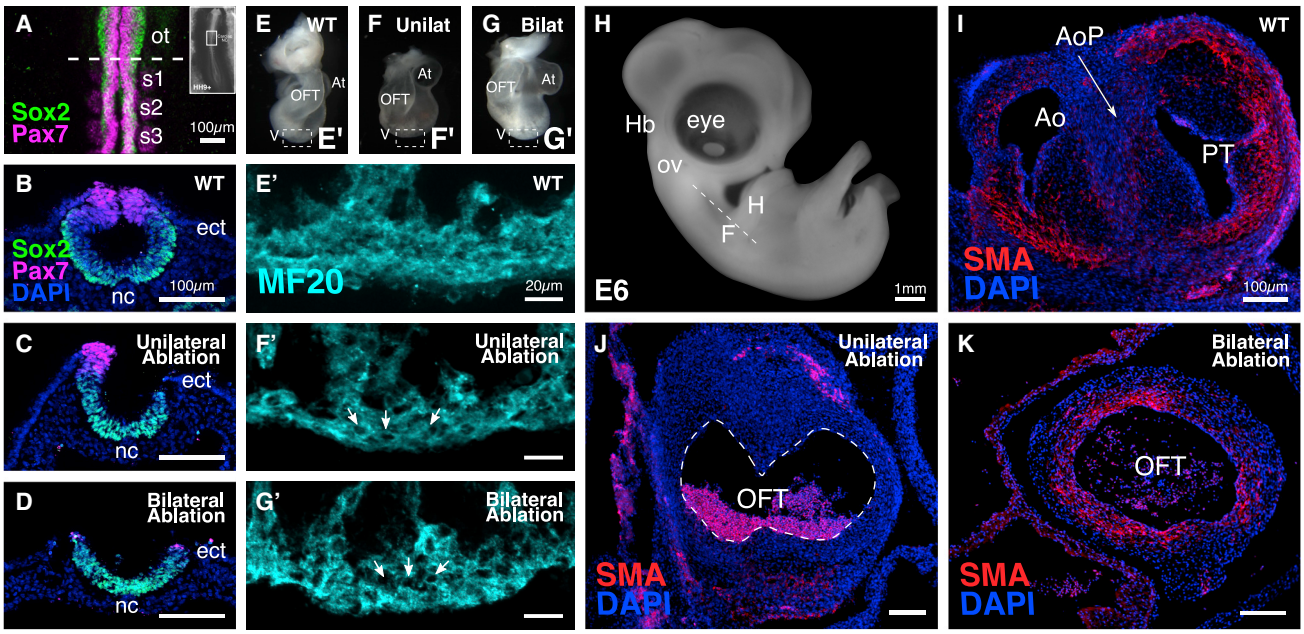

Figure 1. Chick Cardiac Neural Crest Ablation Results in Cardiovascular Abnormalities

(A) Dorsal view of a whole-mount stage HH9+ embryo (inset). Cardiac domain stained with neural crest marker Pax7 (magenta) and neural tube marker Sox2 (green). Dotted line indicates level of sections in (B–D).

(B) Transverse section through A shows cardiac neural crest residing in the dorsal neural tube in wild-type embryo.

(C and D) Transverse section through embryos after unilateral (C) and bilateral (D) dorsal neural fold ablation.

(E–G) Ventral view of E3 wild-type (E), unilaterally ablated (F), and bilaterally ablated (G) primary heart tubes. (E′–G′) Sections through (E–G) stained with the muscle marker MF20 show uniform labeling in wild-type (E′) hearts but patchy expression (arrows) in unilaterally (F′) and bilaterally (G′) ablated embryos.

(H) Whole-mount image of an E6 chick embryo. Dotted line shows angle of sectioning in (I–K).

(I) Cross-section through the outflow tract of a wild-type E6 embryo shows complete septation, with the aorticopulmonary septum (AoP) separating the aorta (Ao) from pulmonary trunk (PT).

(J and K) Unilateral (J) and bilateral (K) cardiac crest ablation results in the failure of outflow tract septation, resulting in a single vessel emerging from the heart. (SMA, red; DAPI, blue) ot, otic placode; s, somites; ect, ectoderm; nc, notochord; At, atrium; V, ventricle; OFT, outflow tract; Hb, hindbrain; ov, otic vesicle; H, heart; F, forelimb; Ao, aorta; PT, pulmonary trunk; AoP, aorticopulmonary septum. See also Figure S1.

Tgif1, functions in a cardiac neural crest subcircuit important for specification and proper outflow tract septation. Finally, we show that ectopic expression of a cardiac-crest-specific subcircuit, comprised of *Sox8*, *Tgif1*, and *Ets1*, is sufficient to reprogram trunk neural crest cells, enabling them to migrate to the heart and rescue the effects of a cardiac crest ablation, which they cannot normally do. Taken together, our results help elucidate the unique genetic properties of the cardiac neural crest in formation and function of the heart. Our results uncover potential target genes involved in cardiovascular birth defects and provide a molecular recipe for generating ectomesenchymal derivatives of the cardiac crest for the purposes of regenerative medicine.

RESULTS

Ablation of the Chick Cardiac Neural Crest Results in Cardiovascular Defects

The cardiac neural crest was described by Kirby and colleagues (Besson et al., 1986; Bockman et al., 1987; Harrison et al., 1995; Kirby et al., 1985; Nishibatake et al., 1987) as arising in the caudal hindbrain (Figures 1A and 1B). Moreover, bilateral ablation of this region in chick embryos at a time corresponding to when the cardiac crest cell fate is specified (Ezin et al., 2009) resulted in improper cardiovascular development. To reproduce and extend cardiac neural crest ablation experiments, we ablated the chick dorsal neural tube adjacent to the caudal hindbrain (Figures 1C and 1D) at Hamilton and Hamburger stage (HH)9–10 (Hamburger and Hamilton, 1951) and allowed embryos to develop until embryonic day (E) 3 or E6. In normal embryos, the primary heart tube exhibited proper elongation and looping dynamics at E3 (Figures 1E and S1A). Staining sections of the heart tube for the myosin heavy-chain marker MF20 revealed uniform filamentous staining throughout the myocardial sleeve (Figure 1E′) of the distal outflow limb. At E6, the aorticopulmonary septum of control embryos developed normally (Figure 1I) with the aorta connected to the left ventricle and pulmonary trunk connected to the right. In contrast, bilaterally ablated embryos had an uneven distribution of MF20 in the distal outflow limb at E3 (Figure 1G′) and a complete lack of septation of the outflow tract at E6, characteristic of severe PTA (Figure 1K).

Next, we unilaterally ablated either the right (n = 9) or left (n = 8) dorsal neural tube, leaving the contralateral side intact (Figures 1C and 1D). At E3, the primary heart tube appeared ‘‘bulbous’’ with a shortened and straighter outflow tract compared with the control group (Figures 1F and 1G); no differences were noted between right or left cardiac neural fold ablations. At E6, removal of the cardiac neural folds from the right side caused PTA (n = 4/9 embryos) (Figure 1J), albeit not as severe as the phenotype

observed following bilateral ablation. Notably, all embryos with an outflow tract septation defect following unilateral ablation had outflow tract cushions that failed to fuse in the middle, suggesting that a critical cardiac neural crest cell number is necessary to form the aorticopulmonary septum. In three cases, we observed double outlet right ventricle (DORV), another phenotype commonly associated with cardiac crest perturbations. In contrast to right side unilateral ablation, removal of the left dorsal neural tube resulted in DORV as the predominant phenotype (n = 6/8) (Figure S1B), with one embryo having PTA. These results raise the intriguing possibility that differences exist in the cardiovascular contributions of cardiac crest cells from different sides of the neural tube. Together, our results suggest that a bilateral cardiac neural crest contribution is necessary for proper outflow tract septation, and that unilateral extirpation of the caudal hindbrain is sufficient to cause cardiovascular anomalies.

Population-Level Transcriptome Analysis Reveals Genes Enriched in the Cardiac Neural Crest

To identify molecular mechanisms underlying the cardiac crest's unique developmental potential to contribute to the cardiovascular system, we turned to a comparative transcriptomics approach to identify transcription factors enriched in the cardiac relative to trunk crest populations. To this end, we used the FoxD3-NC2 (Simões-Costa et al., 2012) enhancer that drives reporter expression in cardiac crest at HH12 (Figure 2A) and later in the trunk neural crest (Figure 2B). Dissecting embryos at different axial levels and developmental time points enabled isolation of pure migrating cardiac and trunk neural crest populations by fluorescence-activated cell sorting (FACS). Following library preparation, sequencing, and data analysis, we identified 474 genes upregulated in cardiac compared with trunk neural crest population (Figure 2C; Table S1). Quality control on the sequenced libraries showed that the data were good quality (Figures S1C and S1D).

Next, we focused on transcription factors that were significantly upregulated in cardiac versus trunk crest (Figure 2C′). We identified some transcription factors that were previously known to be expressed and/or functionally relevant in cardiac crest development, including v-ets avian erythroblastosis virus e26 oncogene homolog 1 *(Ets1)* (Gao et al., 2010), MAF BZIP transcription factor B (*MafB*), and transcription factor AP-2 beta (*Tfap2b*) (Tani-Matsuhana et al., 2018) (Figures 2D–2F). Others, such as TGFB-induced factor homeobox 1 (*Tgif1*), SRY box transcription factor 8 (*Sox8*), NACC family member 2 (*Nacc2*), and MAF BZIP transcription factor K (*MafK*), were transcription factors not previously ascribed to the cardiac neural crest. Their expression in the migrating cardiac crest was validated using *in situ* hybridization (Figures 2G–2I). Next, we compared genes enriched in cardiac crest with those previously shown to be enriched in cranial crest (Simoes-Costa and Bronner, 2016). While some genes were shared with the cranial (e.g., *Ets1*, *Sox8*, and *Tfap2b*), other genes were unique to the cardiac crest stream (e.g., *Tgif1*, *MafK*, and *Nacc2*), thus identifying previously uncharacterized cardiac axial level-selective transcription factors.

scRNA-Seq Reveals Heterogeneity in Migrating Cardiac Crest

Next, we turned to scRNA-seq to deeply profile individual cardiac neural crest cells. To this end, we labeled cardiac crest cells as described above and isolated 156 single cells using FACS. The libraries containing each barcoded cell were multiplexed and sequenced to obtain over 100,000 reads per cell. Following alignment, filtering, and normalization, we recovered high-quality data for 149 single cells (Figures S1E–S1G).

Principal component analysis (PCA) followed by uniform manifold approximation and projection (UMAP) revealed the presence of 4 distinct clusters (C1, C2, C3, and C4) within the migrating cardiac crest population, suggesting heterogeneity between clusters (Figure 2J). Bona fide migratory crest markers *Sox10* and *FoxD3* were less abundant in C3 compared with C1, C2, and C4 (Figures 2J′ and 2J″), suggesting that a subset of migrating cardiac crest cells may already be downregulating an early neural crest program, perhaps indicating fate restriction. To further explore these differences, we performed Gene Ontology (GO) term enrichment analysis of genes that were differentially upregulated in each cluster (Figure 2K) and found that biological processes, such as heart development and circulatory system development, were primarily associated with C1 and C2 ($p < 0.05$; Fisher's exact test). C3 was associated with positive regulation of smooth muscle cell proliferation and muscle cell differentiation, consistent with reduced expression of bona fide neural crest markers. Similarly, C4 was associated with ephrin receptor signaling and central nervous system development, supporting a neuronal identity. C1 and C2 were transcriptionally similar to each other (Figure 2L) apart from a subtle increase in expression of cell proliferation genes, such as *Kpna2* and *Cdc20* in C2. In contrast, we found a significant enrichment of ectomesenchymal cell state markers, such as *Twist1*, *Prrx1*, and *Acta2* in C3, suggesting that cells in this cluster have acquired a restricted ectomesenchymal cell state at the expense of a multipotent neural crest identity. Furthermore, C4 had increased expression of Schwann cell markers, such as *EphA4*, *Krox20*, and *Nrip3*, along with bona fide crest markers, such as *Sox10*, *Ets1*, and *FoxD3*. Based on marker genes, we ascribed the following identities to the single-cell subclusters: progenitor cardiac crest (C1, C2), ectomesenchymal cardiac crest (C3), and Schwann-cell-like (C4). Interestingly, hierarchical clustering with labeled UMAP cluster identity showed that a subset of progenitor cardiac crest cells was affiliated with the ectomesenchymal group, suggesting that we captured single cells that were transitioning from a neural crest progenitor to an ectomesenchymal-like state. We further explored the potential relationships between subpopulations using Monocle (Figures 2M and 2N). Unsupervised clustering along the pseudotime trajectory demonstrated a gradual transition from cells in cluster C1 (progenitor) to proliferating (C2), Schwann cell-like (C4), and ectomesenchymal (C3) cardiac crest (Figure 2M). Taken together, these results suggest cellular heterogeneity within early migrating cardiac crest populations.

To test whether our single-cell data, pooled together, recapitulated the cardiac neural crest transcriptomic profile obtained from bulk RNA sequencing, we compared the relative abundance of transcripts as measured by fragments per kilobase of exon per million fragments mapped (FPKM). The genes enriched in the two datasets were positively correlated, with a Pearson's correlation coefficient of 0.85 (Figure S1H). Using markers identified and validated at the population level, we looked for their distribution of expression in the scRNA-seq data (Figure S1I). As expected, the expression of cardiac crest markers *Ets1*, *MafB*, *Tfap2b*, *MafK*, *Nacc2*, *Sox8*, and *Tgif1* was uniformly distributed across C1, C2, and C4, with the latter four also

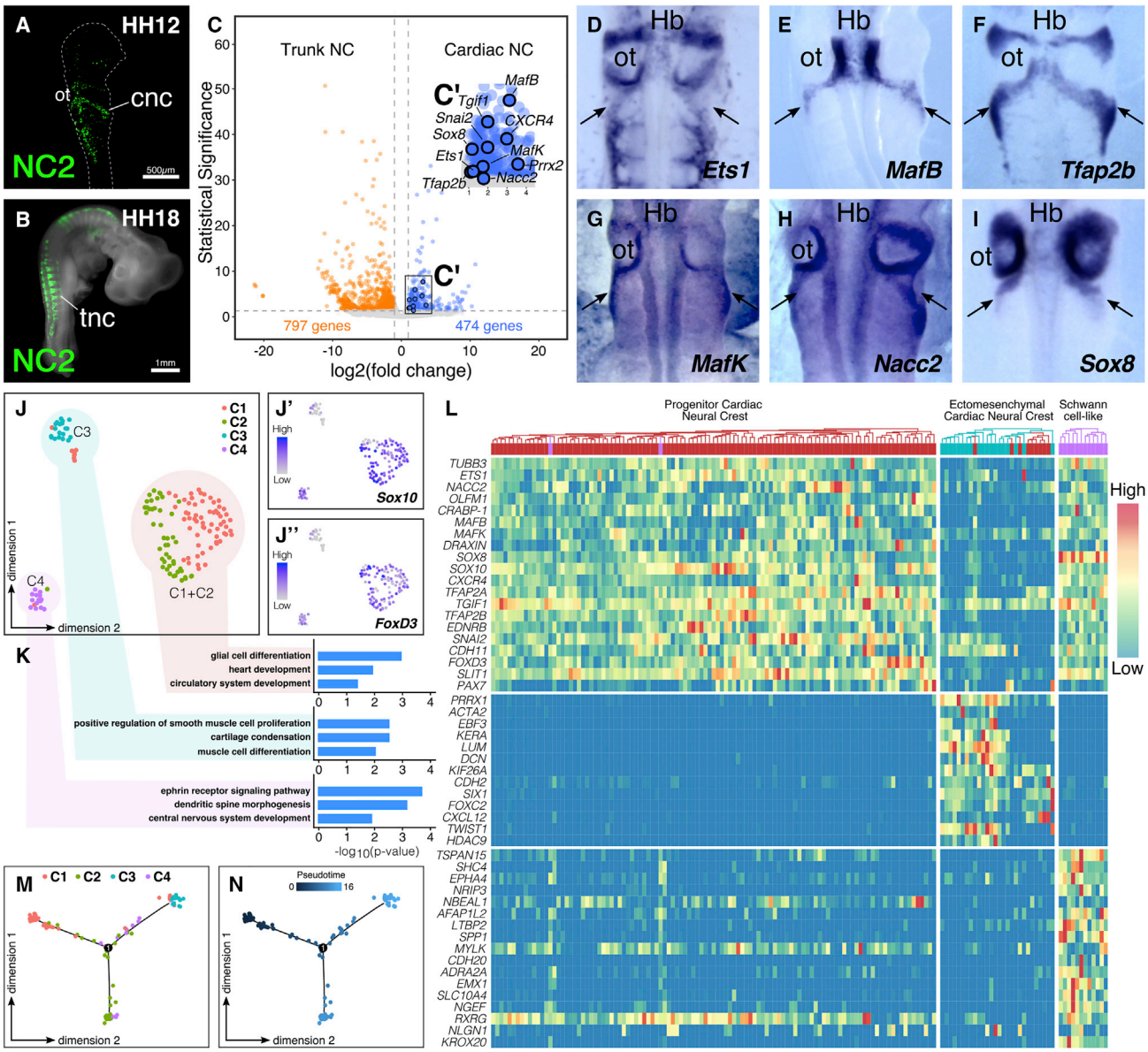

Figure 2. Bulk and Single-Cell Transcriptional Profiling of Cardiac Neural Crest

(A and B) Pure populations of cardiac or trunk neural crest cells labeled with the FoxD3-NC2 enhancer were isolated using FACS at HH12 (A) and HH18 (B), respectively.

(C and C′) Volcano plot showing fold change and significance of genes enriched in cardiac and trunk neural crest (logFoldChange > 1). Transcription factors examined for expression in migrating cardiac crest are highlighted in (C′).

(D–I) *In situ* hybridization of HH12 embryos shows expression of *Ets1* (D), *MafB* (E), *Tfap2B* (F), *MafK* (G), *Nacc2* (H), and *Sox8* (I) in migratory cardiac crest (dorsal view, arrows).

(J) UMAP plot depicting clustering of 149 single cardiac neural crest cells that were profiled using smart-seq V2. (J′ and J″) Clusters C1 and C2 exhibit high expression of neural crest markers *Sox10* (J′) and *FoxD3* (J″) and differed subtly in the expression of proliferation genes.

(K) GO term analysis on differentially upregulated genes in each cluster confirms identity of each subpopulation within the migrating cardiac crest (Fisher's exact test, adjusted $p < 0.05$).

(L) Heatmap illustrating hierarchical clustering of 149 single cells (columns) and expression levels of selected neural crest, ectomesenchymal, and neuronal genes (rows). A few cells from the cardiac crest progenitor clusters C1 and C2 (magenta) grouped together with cells from the ectomesenchymal cluster C3 (blue).

(M and N) Pseudotime analysis (M) on migratory cardiac crest cells. Cells are labeled according to their pseudotime values (N). ot, otic vesicle; cnc, cardiac neural crest; tnc, trunk neural crest; Hb, hindbrain. See also Figure S1; Table S1.

similarly expressed in C3. Together, these results demonstrate that the four subclusters reflected the profile observed in the bulk cardiac crest dataset.

Transcription Factor *Tgif1* Is Required for Cardiac Neural Crest Specification

With an eye toward finding transcription factor(s) expressed at the onset of cardiac crest specification, we analyzed spatiotemporal expression patterns and were particularly intrigued by *Tgif1* due to its selective expression in the delaminating cardiac crest at HH10 (Figures 3A, 3B, and 3E), the time at which cardiac crest fate is determined (Ezin et al., 2009). *Tgif1* expression was first observed at stage HH9+ (Figure 3A) in the dorsal neural tube between the otic vesicle and the third somite, overlapping with the cardiac neural crest territory. After delamination at HH10 (Figures 3B and 3E), *Tgif*1 expression was retained in migrating cardiac crest cells coexpressing neural crest marker HNK-1 (Basch et al., 2006) at HH12 (Figures 3C, 3D, 3F, and 3F′).

We next examined the role of *Tgif1* in cardiac crest development. To this end, we used a CRISPR-Cas9-mediated strategy (Gandhi et al., 2017) to knock out *Tgif1* in early chick embryos. We designed two guide RNAs (gRNAs), one targeting the splice acceptor site of the second exon, and the second one targeting the third exon (Figure S2A). To test if gRNAs targeting *Tgif1* were sufficient to knock out its expression, we electroporated the right side of gastrula stage embryos with expression constructs for Cas9, *Tgif1* gRNAs, and H2B-RFP and the left side with control reagents and GFP (Figures 3G and 3H). Embryos were cultured *ex ovo* until HH12 and assayed for expression of *Tgif1* by *in situ* hybridization. As expected, these embryos exhibited nearly complete loss of *Tgif1* (Figure 3I) on the experimental side, validating our approach. Furthermore, knockout of *Tgif1* resulted in a notable reduction in expression of other cardiac crest markers like *Tfap2B*, *MafB*, *Nacc2*, *Ret*, and *CXCR4* (Figures 3J–3N). Interestingly, while expression of the pan-neural crest markers *Sox10* and *FoxD3* was reduced on the Tgif1 knockout side, the number of cells migrating away from the neural tube was similar, albeit in disorganized migration streams (Figures S2B and S2C). These data suggest that *Tgif1* plays a pivotal role in the cardiac crest gene regulatory network.

Tgif1 Is Necessary for Proper Outflow Tract Septation

Given its importance in early cardiac crest development, we asked if *Tgif1* is necessary for proper outflow tract septation using a grafting approach where the dorsal neural tube adjacent to the hindbrain of GFP$^+$ control or *Tgif1* knockout embryos was either unilaterally or bilaterally grafted into wild-type embryos (Figure 3O).

As right unilateral cardiac neural fold ablation produces PTA (Figure 1H), we first asked whether unilateral knockout of *Tgif1* was sufficient to cause septation defects. To this end, we electroporated Cas9, *Tgif1* gRNAs, and H2B-RFP on the right side of gastrula stage transgenic embryos and cultured them *ex ovo* until HH9+; control embryos were electroporated with expression constructs for Cas9, control gRNA, and H2B-RFP. Chimeras were developed until E6, the stage by which outflow tract septation in chick embryos is complete. Transverse sections through control chimeras confirmed that the outflow tract was properly septated, with GFP$^+$ cardiac crest cells condensed in the septum (Figure 3P; n = 2/2), replicating previous results of quail-chick chimeras (Kirby, 1989; Kirby et al., 1985). Next, we repeated this experiment with unilateral grafting of the cardiac neural fold from a *Tgif1* knockout transgenic embryo. The results show that this also results in a fully septated outflow tract, albeit with significantly reduced number of GFP$^+$ cells in the septum (Figure S2D; n = 4/4). Thus, the presence of the contralateral host cardiac crest together with a reduced number of transgenic cells appears to be sufficient to compensate for the unilateral loss of *Tgif1*.

As its unilateral loss was not sufficient to cause abnormalities, we tested the effects of bilateral *Tgif1* loss of function using bilateral neural fold grafts from *Tgif1* knockout transgenics. Remarkably, in E6 embryos, the outflow tract failed to septate, resulting in a single outflow vessel emerging from the heart (Figure 3Q; n = 3/3), despite the migration of transgenic cells into the outflow tract. GFP$^+$ cells were observed in other known derivatives of the cardiac crest, such as the left and right internal and external carotid arteries, demonstrating that outflow tract defects did not result from improper graft incorporation (Figure S2E). Taken together, the results show that *Tgif1* expression in cardiac neural crest cells is necessary for proper outflow tract septation.

We confirmed that *Tgif1* was not expressed in trunk neural crest by using hybridization chain reaction (HCR) against *Sox10*, *FoxD3*, and *Tgif1* in a HH15 chick embryo (Figure S2F). While *Sox10*, *FoxD3*, and *Tgif1* expression overlapped in cardiac crest cells invading the circumpharyngeal ridge, *Tgif1* transcripts were absent from migrating trunk neural crest cells (Figures S2G and S2H). We next asked if *Tgif1* was sufficient to confer "cardiac-like" characteristics onto other axial levels but found that ectopic expression of *Tgif1* alone failed to activate the Sox10E2 cranial and cardiac neural crest enhancer (Betancur et al., 2010) in the trunk neural crest, used here as a readout for cardiac identity (Figures S2I–S2K). This suggested that other factors might work synergistically with *Tgif1* for acquisition of cardiac crest fate. As we previously reported that minimum of three transcription factors were required to reprogram trunk neural crest to a cranial crest identity (Simoes-Costa and Bronner, 2016), we broadened our search to identify other putative cardiac neural crest subcircuit genes that might work in concert with *Tgif1*.

HCR and scRNA-Seq Reveal Coexpression of *Tgif1* with *Ets1* and *Sox8*

We were able to eliminate several candidate genes that were not yet expressed in delaminating and/or early migrating cardiac crest cells (Figure S3A). However, *Ets1* caught our attention as its loss causes ventricular septal defects, commonly associated with defects in cardiac crest development (Gao et al., 2010; Ye et al., 2010). In addition, SoxE transcription factors *Sox8/9/10* are necessary for initiation of neural crest formation at all axial levels (O'Donnell et al., 2006). Among the family of SoxE factors, *Sox8* was significantly enriched in cardiac relative to trunk neural crest. We first performed HCR using probes for *Sox8*, *Tgif1*, and *Ets1* on HH12 chick embryos to test their coexpression (Figure 4A). The results reveal overlapping expression of *Ets1*, *Sox8*, and *Tgif1* in migrating cardiac crest cells (Figures 4B and 4B″) at single-cell resolution, with the three genes overlapping in the post-otic stream of migrating neural crest cells (Figures S3B–S3E).

To further explore their coexpression at the single-cell level, we probed individual cells from our scRNA-seq dataset. Among the four subpopulations, subclusters C1 and C2 had signatures

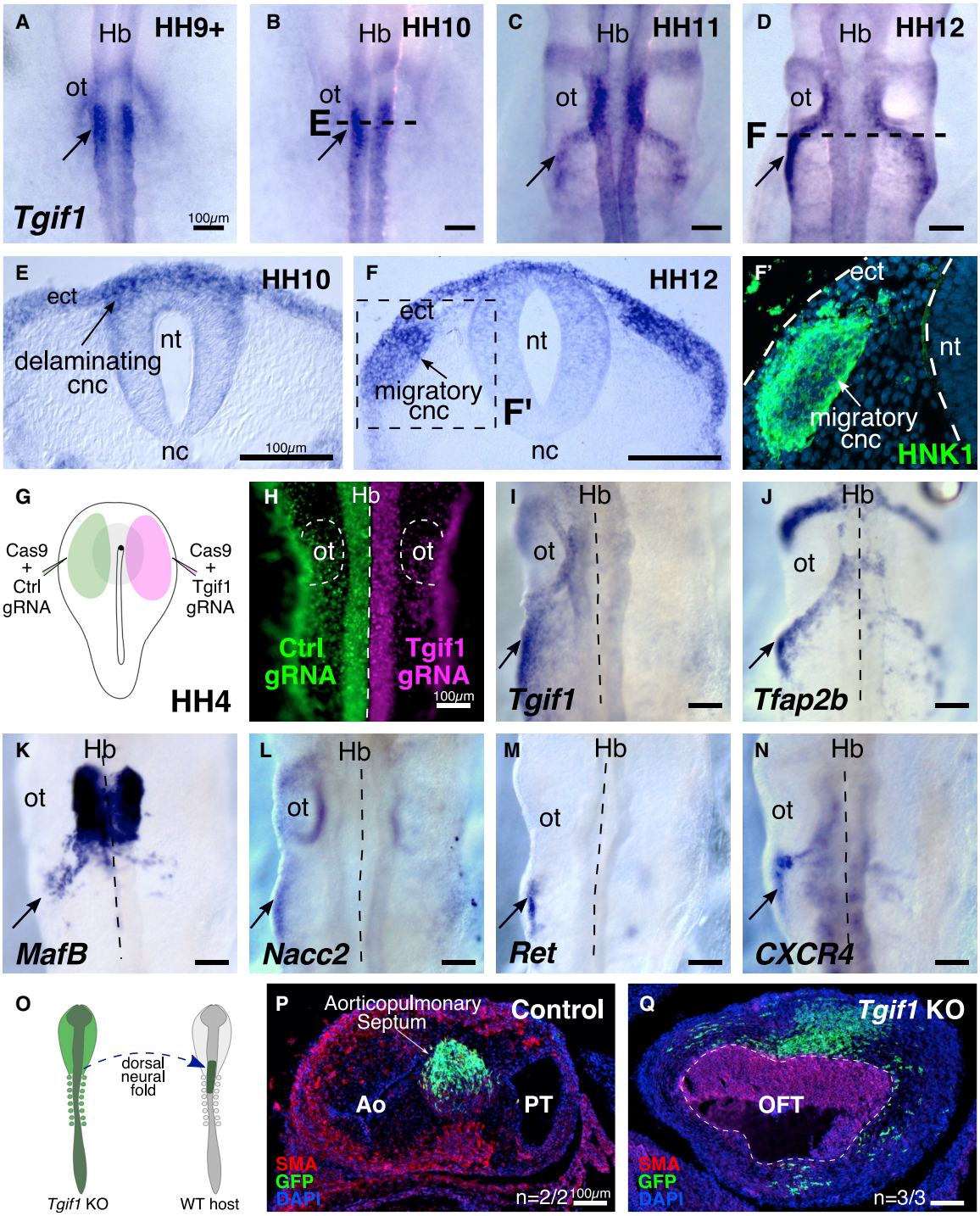

Figure 3. *Tgif1* Is Critical for Cardiac Neural Crest Specification and Outflow Tract Septation

(A–D) Spatiotemporal expression pattern of *Tgif1* in cardiac neural crest at stages HH9+ (A), HH10 (B), HH11 (C), and HH12 (D) (dorsal view, arrows).

(E) Transverse section through (B) shows *Tgif1* expression in delaminating cardiac crest cells in the dorsal neural tube.

(F and F′) Transverse section through (D) shows *Tgif1* expression in migrating cardiac crest, which overlaps with the expression of the neural crest marker HNK1 (F′).

(G) Diagram depicting *ex ovo* electroporation strategy for *Tgif1* knockout in gastrula stage embryos. (H) An embryo transfected with gRNAs targeting *Tgif1* (magenta) and control gRNA (green) (dorsal view).

(I–N) Following CRISPR-Cas9-mediated knockout of *Tgif1*, expression of *Tgif1* (I), *Tfap2B* (J), *MafB* (K), *Nacc2* (L), *Ret* (M), and *CXCR4* (N) was significantly reduced (dorsal view). Arrows indicate normal gene expression on control side.

(legend continued on next page)

characteristic of progenitor cardiac crest cells. By visualizing the expression of the three genes on a UMAP plot (Figures 4C–4E and S3F–S3K), we found overlapping expression of *Tgif1, Sox8*, and *Ets1* in 93% of the cells in the two cardiac neural crest progenitor clusters (Figure 4F), suggesting that they could function as a cardiac-crest-specific subcircuit. Of note, downstream cardiac crest transcription factors *Tfap2B*, *MafB*, *Nacc2*, and *Ret* were also coexpressed with *Tgif1, Sox8*, and *Ets1*.

Sox8, Tgif1, and *Ets1* Comprise a Transcriptional Cascade Important for Cardiac Neural Crest Identity

To explore regulatory relationships between *Sox8, Tgif1*, and *Ets1*, we first performed HCR (Figures 4G–4I) to establish their temporal order of expression in the cardiac crest. The results show that *Sox8* turns on first at HH9, followed by *Tgif1* at HH9+ and *Ets1* at HH10+ (Figures 4J and 4K). Given this putative hierarchy, we examined their functional relationships within a subcircuit by individually knocking out *Sox8, Tgif1*, or *Ets1* using CRISPR-Cas9. To this end, we performed *ex ovo* electroporation of expression constructs for Cas9, gRNAs targeting *Sox8*, *Tgif1*, or *Ets1* (Figure S2A) and H2B-RFP on the right side of gastrula stage embryos; the left side was transfected with control reagents. Embryos were cultured *ex ovo* until HH11 then assayed for expression of the three factors using HCR.

Sox8 knockdown resulted in loss of both *Tgif1* and *Ets1* (Figures 5A, 5E, and 5J), suggesting that Sox8 forms the uppermost node of this transcriptional subcircuit. On the other hand, knockout of Tgif1 resulted in reduction of *Ets1* expression (Figure 5K) but no noticeable effect on *Sox8* (Figure 5B). Finally, loss of Ets1 had no effect on either *Sox8* (Figure 5C) or *Tgif1* (Figure 5G) in the premigratory neural crest, albeit *Sox8* levels were reduced in the otic vesicle, suggesting that *Ets1* might be a functional input into *Sox8* in the ear but not cardiac crest. To further explore the epistatic nature of these regulatory relationships, we asked if *Ets1* expression could be rescued after *Sox8* knockout by exogenously expressing *Tgif1*. To test this, we removed *Sox8* on the right side of gastrula stage embryos using CRISPR-Cas9 as described above and concomitantly ectopically expressed *Tgif1*. Overexpression of *Tgif1* was sufficient to partially rescue the levels of *Ets1*, even though the level of *Sox8* was notably diminished (Figures 5D and 5D′).

Next, we asked if these regulatory linkages might result from direct interactions. To this end, we searched for putative transcription-factor-binding sites in enhancers that mediated expression of *Tgif1* and *Ets1* in cardiac crest. For *Ets1*, we used a previously published enhancer that recapitulates *Ets1* expression in the cranial and cardiac neural crest (Barembaum and Bronner, 2013). For *Tgif1*, we identified an enhancer that was evolutionarily conserved across several vertebrate species (Figures S4A–S4C) and drove reporter expression in a manner that recapitulated that of *Tgif1*. We then identified and mutated putative-binding sites for *Sox8* in the Tgif1 enhancer (Tgif1-ΔSox8) and for *Tgif1* in the Ets1 enhancer (Ets1-ΔTgif1). Mutant and wild-type enhancers driving GFP were electroporated on the right or left side of gastrula stage embryos, respectively. H2B-RFP was electroporated on both sides as a transfection control (Figures 5H and 5M). The results show that the loss of Sox8- and Tgif1-binding sites was sufficient to reduce Tgif1 and Ets1 enhancer activity in the cardiac crest, respectively (Figures 5I and 5N). Interestingly, the Ets1-ΔTgif1 mutant enhancer retained activity in cranial neural crest (Figure 5N), suggesting its differential regulation in cranial versus cardiac crest. Taken together, our results suggest a regulatory cascade consistent with the sequential expression pattern of *Sox8*, *Tgif1*, and *Ets1*, with the former two working together in the premigratory cardiac crest and regulating the activity of *Ets1* in the migratory neural crest (Figure 5O). Using the pseudotime lineage trajectory defined earlier (Figure 5P), we plotted the relative expression pattern of our cardiac crest subcircuit genes on the trajectory map (Figures 5Q–5S). Although expression of all three genes was high in both progenitor and proliferative cardiac crest cells, both *Sox8* (Figure 5Q) and *Ets1* (Figure 5S) were downregulated as the cells transitioned into an ectomesenchymal state. The expression of *Tgif1* (Figure 5R) was relatively unchanged, strengthening our hypothesis that *Tgif1* is important for the formation of ectomesenchymal derivatives of cardiac crest.

Based on these results, we hypothesized that these three genes may comprise a "cardiac neural crest subcircuit" that might confer cardiac-like identity onto other neural crest populations. To examine downstream genes associated with a "cardiac-like" crest identity, we ectopically expressed *Sox8*, *Tgif1*, and *Ets1* along with the Sox10E2 reporter construct as "reprogramming readout" into the trunk neural crest of HH10 embryos (Figures S4D and S4E). After RNA-seq of enhancer-expressing-sorted cells, we identified genes upregulated in the reprogrammed neural crest cells compared with unelectroporated trunk crest (Figure S4F). Examples of upregulated genes included "cardiac crest markers" like *Nacc2, Ret*, and *Cdh11*, that were otherwise absent from trunk crest cells. On the other hand, key trunk neural crest genes including *HoxA6, Dll1*, and *Mitf* were downregulated in the reprogrammed population (Figure 5T). To validate the observed gene expression differences between reprogrammed and wild-type trunk neural crest cells, we electroporated the right side of gastrula stage embryos with expression constructs for *Sox8*, *Tgif1*, and *Ets1*, and the left side with an equal concentration of H2B-RFP (Figure 5U). As expected, expression of the cardiac crest subcircuit elicited ectopic expression of *Nacc2* (Figure 5V) in both cranial neural crest and the naive ectoderm. In contrast, overexpression of the three transcription factors in the trunk neural tube of HH10 (Figure 5W) led to reduction of the trunk neural crest gene *Hes6* at HH18 on the experimental (right) compared with control side (left) (Figure 5X), suggesting that neural crest identity was altered to be cardiac-like at the expense of the original trunk-like signature. Taken together, these results suggest that the

(O) Experimental strategy to investigate the role of *Tgif1* in outflow tract septation. Cardiac neural folds from a transgenic embryo where *Tgif1* was bilaterally knocked out at the gastrula stage were grafted in place of the ablated cardiac crest in a stage-matched HH9+ wild-type host.
(P) Cardiac crest cells from control gRNA-electroporated transgenic graft are observed within the condensed mesenchyme of a properly septated outflow tract.
(Q) The OFT of embryos grafted with the *Tgif1* knockout cardiac neural folds failed to septate. Hb, hindbrain; ot, otic placode; ect, ectoderm; nt, neural tube; nc, notochord; cnc, cardiac neural crest; Ao, aorta; PT, pulmonary trunk; OFT, outflow tract. See also Figure S2.

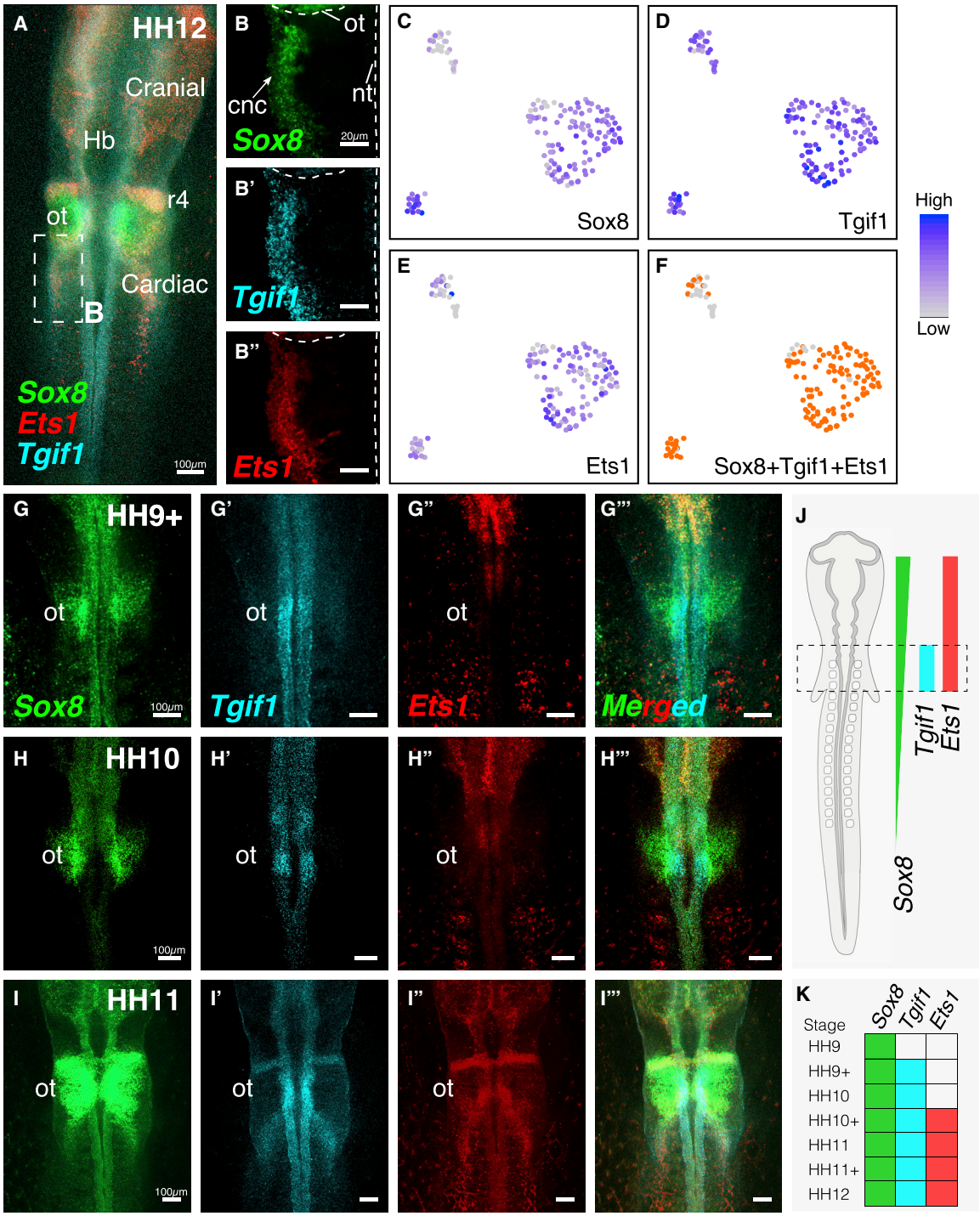

Figure 4. *Tgif1* Is Coexpressed with *Sox8* and *Ets1* in Migrating Cardiac Neural Crest

(A–B″) HCR against *Sox8* (B), *Tgif1* (B′), and *Ets1* (B″) shows their overlapping expression in the migrating cardiac crest cells.

(C–F) Expression levels of *Sox8* (C), *Tgif1* (D), and *Ets1* (E) in individual cardiac crest cells following smart-seq-v2-based single-cell profiling. In progenitor cardiac crest clusters, the three genes had overlapping expression (orange) in 93% of the cells (F).

(G–I) Spatiotemporal expression pattern of *Sox8* (G, H, I), *Tgif1* (G′, H′, I′), and *Ets1* (G″, H″, I″) overlaps in the cardiac crest region (G‴, H‴, I‴) between stages HH9+ and HH12 (dorsal view).

(J) Schematic diagram of HH12 embryo shows overlapping expression domains of *Tgif1*, *Ets1*, and *Sox8* in the cardiac neural crest.

(K) The hierarchy of temporal expression dynamics of cardiac crest subcircuit genes from HH9 to 12. ot, otic placode; Hb, hindbrain; r4, rhombomere 4 migrating crest stream; nt, neural tube; cnc, cardiac neural crest. See also Figures S2 and S3.

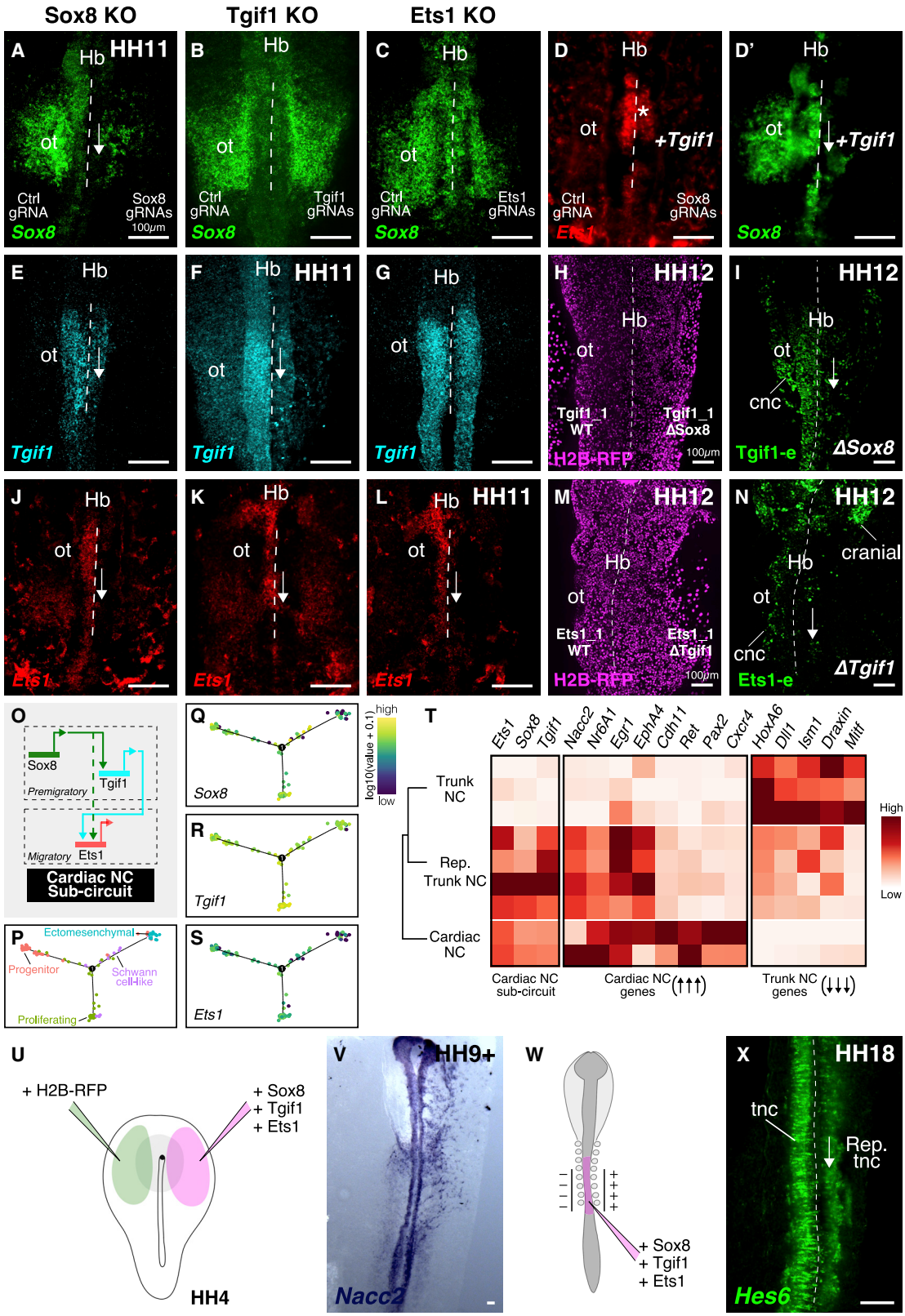

Figure 5. *Sox8*, *Tgif1*, and *Ets1* Comprise a Transcriptional Cascade Important for Cardiac Crest Identity

(A–N) Dorsal view of HH11 embryos where *Sox8* (A, E, and J), *Tgif1* (B, F, and K), or *Ets1* (C, G, and L) was knocked out on the right side at gastrula stage. *Sox8* knockout resulted in loss of *Tgif1* (E) and *Ets1* (J); *Tgif1* knockout resulted in reduced *Ets1* (K) but no noticeable change in *Sox8* (B); *Ets1* knockout had no effect on

(legend continued on next page)

combination of *Tgif1*, *Ets1*, and *Sox8* was sufficient to alter the character of neural crest cells from other axial levels, imbuing transfected cells with cardiac-crest-like identity.

Reprogrammed Trunk Neural Crest Cells Exhibit Cardiac-Crest-like Migratory Behavior

Cardiac neural crest cells emerge in three distinct streams from the dorsal neural tube adjacent to rhombomeres 6, 7, and 8 and exhibit chain migration similar to cranial crest cells. The rostral-most stream of the cardiac crest follows a dorsolateral pathway of migration, forming a distinctive arc-like pattern, as shown by FoxD3-NC2 enhancer-driven GFP expression at HH12 (Figure 2A). These cells eventually migrate into the circumpharyngeal ridge, where they pause while the branchial arches form. Once developed, the cardiac crest cells continue their migration and populate branchial arches III, IV, and VI, with some contributing to the satellite cells that surround neurons of the nodose and jugular ganglion of the vagus nerve after 2 days.

Given that overexpression of the cardiac crest subcircuit resulted in altered neural crest molecular identity, we next examined the long-term effects of expressing this cardiac crest subcircuit in the trunk neural crest. To this end, we electroporated expression constructs for *Sox8, Tgif1*, and *Ets1* into the trunk neural tube of HH10 transgenic GFP$^+$ embryos *in ovo*. The *Sox8* construct contains a *cis*-internal ribosome entry site (IRES) allowing the expression of the nuclear fluorescent protein H2B-RFP, used as a marker for electroporation efficiency. These ''donors'' were incubated at 37°C for 12 h, after which the dorsal neural tube caudal to somite 10 was surgically removed and unilaterally grafted in place of the cardiac neural fold in wild-type HH9+ host embryos. As a control, unperturbed cardiac neural fold or trunk neural fold was grafted instead (Figure 6A). To confirm that the homochronic, homotopic graft extracted from the donor embryo was successfully incorporated in the host embryo, we implanted the dorsal neural tube from the trunk of a GFP embryo electroporated with expression constructs for the cardiac crest subcircuit genes (Figure 6B). Chimeras were given 10 min to recover following surgery and incubated for 1 h at 37°C prior to fixation and sectioning. Transverse cross-sections through the hindbrain (Figures 6B′–6B‴) confirmed that the graft healed efficiently and was properly incorporated in the host.

To assess effects on cell migration, we allowed chimeras to develop for 2 days. We first analyzed the ''control'' group grafted with unperturbed GFP$^+$ cardiac neural folds in whole-mount and transverse sections. Consistent with results from quail-chick chimeras, GFP$^+$ cardiac crest cells that emerged adjacent to somite 1 and 2 migrated into branchial arch IV (Miyagawa-Tomita et al., 1991) (Figure 6C; n = 3/3) and formed satellite cells of the nodose vagal ganglia (Figures 6F and 6F′). However, when unperturbed GFP$^+$ trunk neural fold was grafted in place of the cardiac neural fold of wild-type hosts, the grafted cells delaminated from the neural tube but exhibited restricted migration (Figure 6D; n = 3/3), resulting in failure to invade branchial arch IV (Figures 6G and 6G′). Moreover, the neurons of the nodose ganglion, otherwise derived from the post-otic placodal ectoderm (Narayanan and Narayanan, 1980), were malformed compared with those of control embryos, consistent with a previously reported cardiac crest ablation phenotype (Kuratani et al., 1991). Thus, trunk neural crest cells failed to substitute for ablated cardiac neural folds as previously published (Harrison et al., 1995; Kirby, 1989).

Importantly, unilaterally grafted ''reprogrammed'' trunk neural folds, electroporated with constructs encoding our cardiac subcircuit genes *Sox8, Tgif1*, and *Ets1*, exhibited ''cardiac crest''-like behavior. These cells migrated into branchial arch IV (Figure 6E; n = 3/3) to form satellite cells of the jugular ganglion of the vagus nerve (Figures 6H and 6H′), similar to normal cardiac crest cells at the 2-day time point. The placodally derived neurons were also evenly distributed. Taken together, these results show that the combined expression of *Tgif1*, *Ets1*, and *Sox8* was sufficient to reprogram trunk neural crest cells to exhibit migration patterns and morphogenesis similar to cardiac crest cells.

Reprogrammed Trunk Neural Crest Acquire Cardiac Ectomesenchymal Potential

Once cardiac crest cells have migrated into the caudal pharynx, a subset condenses around the pharyngeal arch arteries, contributing to the smooth muscle tunica media surrounding these vessels (Bergwerff et al., 1998). While the endothelial cells lining these arteries are mesoderm derived and hence not dependent on cardiac crest for initial development, the cardiac crest plays a vital role in the remodeling of the pharyngeal arch arteries (Bockman et al., 1987), resulting in the formation of the aortic arch, brachiocephalic artery, the carotid arteries, and the subclavian arteries (Hiruma et al., 2002). Ultimately, cardiac crest cells migrate into the outflow tract cushions, where they will condense to form the aorticopulmonary septum. Some of these cells also contribute to the proximal segment of the interventricular septum.

To test whether reprogrammed trunk neural crest cells acquired a developmental potential normally confined to cardiac

either *Sox8* (C) or *Tgif1* (G). (D and D′) Overexpression of *Tgif1* on the right side in *Sox8* knockout embryos (D′) was sufficient to partially rescue *Ets1* expression (D). Mutation of Sox8-binding sites in a Tgif1 enhancer (I) resulted in reduced enhancer activity in the cardiac neural crest on the right side. Mutation of the Tgif1-binding site in an Ets1 enhancer (N) resulted in reduced enhancer activity in cardiac but not cranial neural crest. H2B-RFP (H and M) was used as a transfection control on both sides.

(O) Functional relationships between *Sox8*, *Tgif1*, and *Ets1* in a transcriptional subcircuit based on the results in (A–N).

(P–S) Pseudotime lineage trajectory with each subcluster labeled (P) according to scRNA-seq analysis. Expression of cardiac neural crest subcircuit genes *Sox8* (Q), *Tgif1* (R), and *Ets1* (S) was overlaid on the trajectory.

(T) Heatmap showing changes in gene expression profiles of reprogrammed trunk neural crest compared with wild-type cardiac and trunk crest. Each row is a biological replicate.

(U and V) Dorsal view of an HH9+ embryo where *Tgif1*, *Ets1*, and *Sox8* were overexpressed at gastrula stage on the right side (U). *Ex ovo* culturing of the embryos resulted in ectopic expression of cardiac crest gene *Nacc2* (V) in cranial neural crest and surrounding naive ectoderm.

(W and X) Dorsal view of the trunk neural crest of an HH18 embryo where cardiac crest subcircuit genes were transfected on the right side of the neural tube *in ovo* (W). Expression of trunk neural crest marker *Hes6* was reduced in reprogrammed (right) compared to resident (left) trunk neural crest cells (X). ot, otic placode; Hb, hindbrain; cnc, cardiac neural crest; tnc, trunk neural crest; rep, reprogrammed. See also Figure S4; Table S2.

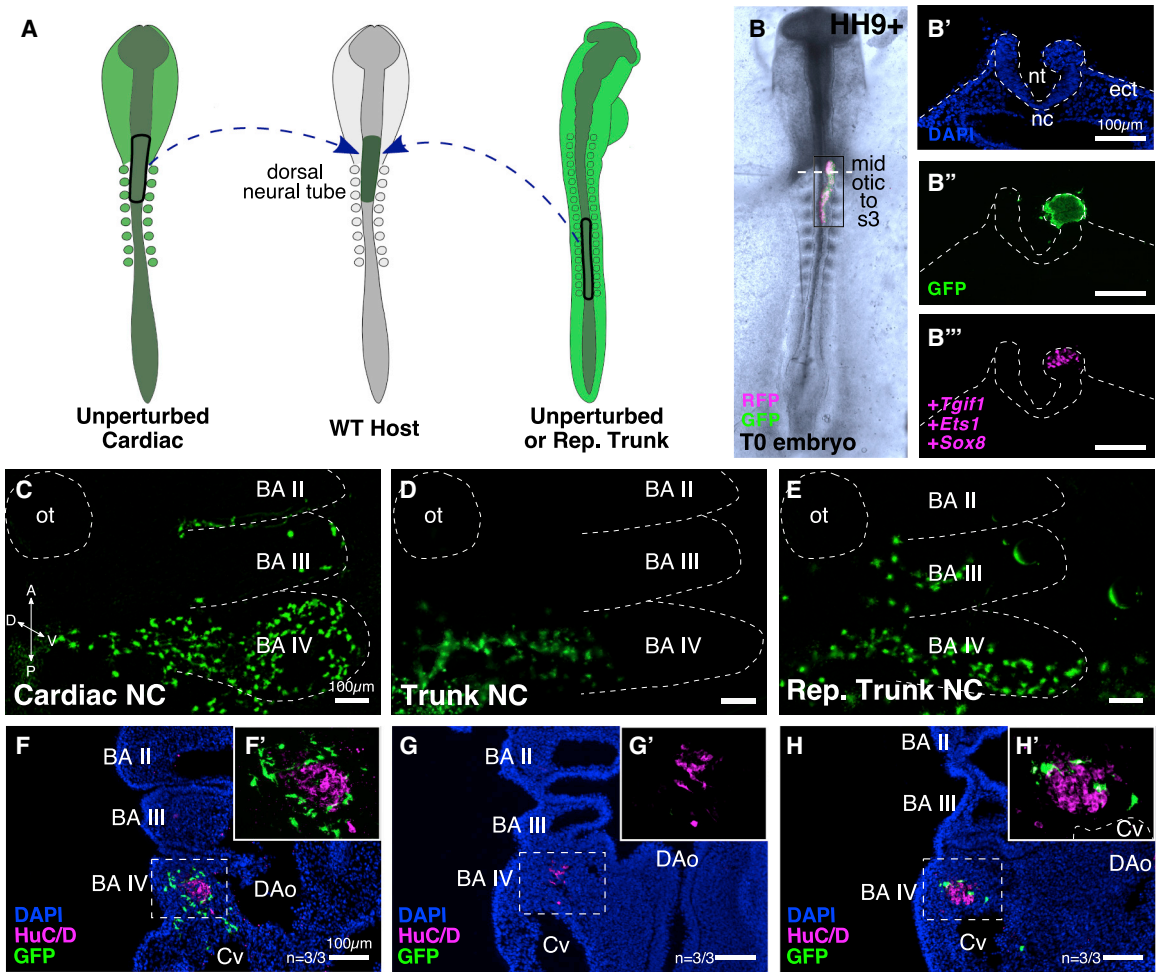

Figure 6. Reprogrammed Trunk Neural Crest Cells Exhibit Cardiac-Crest-like Migratory Behavior

(A) Grafting strategy to test behavior of transplanted cells. Stage-matched cardiac neural fold, unperturbed trunk neural fold, or trunk neural fold reprogrammed by the ectopic expression of *Sox8*, *Tgif1*, and *Ets1* was grafted in place of ablated cardiac neural folds in a wild-type host at HH9+.

(B–B‴) Embryo with a unilateral transgenic implant spanning the cardiac crest domain immediately after grafting (dorsal view). Transverse section through the hindbrain (dotted line) shows successful incorporation (B′) of the GFP+ implant (B″). The graft was electroporated with expression constructs for cardiac neural crest subcircuit genes *Sox8*, *Tgif1*, and *Ets1* (B‴).

(C–H) Whole-mount and cross-section images of chimeras grafted with dorsal cardiac neural folds (C, F, and F′), non-transfected dorsal trunk neural folds (D, G, and G′), and "reprogrammed" dorsal trunk neural folds (E, H, and H′) harvested 2 days post-grafting. Transgenic cells from the cardiac neural fold graft migrated into branchial arches III-IV (C), whereas cells from the trunk neural fold graft exhibited restricted migration (D). Ectopic expression of the cardiac crest subcircuit was sufficient to change the migration behavior of these cells, with transgenic cells populating branchial arches III and IV (E). s, somite; nt, neural tube; ect, ectoderm; nc, notochord; ot, otic vesicle; BA, branchial arches; Cv, cardinal vein; DAo, dorsal aorta.

crest, we analyzed their ability to differentiate into ectomesenchymal derivatives, such as the condensed mesenchyme of the aorticopulmonary septum, tunica media of the branchial arch arteries, and the nodose ganglia (Kirby, 1989; Kirby and Stewart, 1983) (Figures 7A–7C and 7A′–7C′), in comparison with wild-type cardiac and trunk neural fold grafts. First, to validate the contribution of cardiac crest to these different tissues, we unilaterally grafted unperturbed GFP$^+$ neural fold spanning the entire cardiac crest region from a transgenic embryo into a wild-type host and allowed the embryos to develop to E6. Consistent with results obtained with quail-chick chimeras, cardiac crest cells were found in the aorticopulmonary septum (Figures 7A and 7A′), the tunica media surrounding the branchial arch arteries (Figures 7B and 7B′), and neurons and glial cells of the jugular ganglion of the vagus nerve (Figures 7C and 7C′).

In contrast to GFP$^+$ cardiac implants, when unperturbed GFP$^+$ transgenic trunk neural fold was grafted into the cardiac crest region, the host embryos exhibited cardiovascular defects at E6, most notably septation defects of the outflow tract (Kirby, 1989; Nishibatake et al., 1987) (n = 4/5; Figure 7D). Interestingly, the phenotype looked similar to what we observed after unilateral ablations, where the outflow tract cushions had developed but failed to fuse, resulting in PTA (Figure 1H). This suggests that the endogenous cardiac crest from the contralateral side failed to compensate for complete unilateral loss of cardiac neural folds. One embryo exhibited DORV, another similarity observed to that occurring after unilateral cardiac crest ablation.

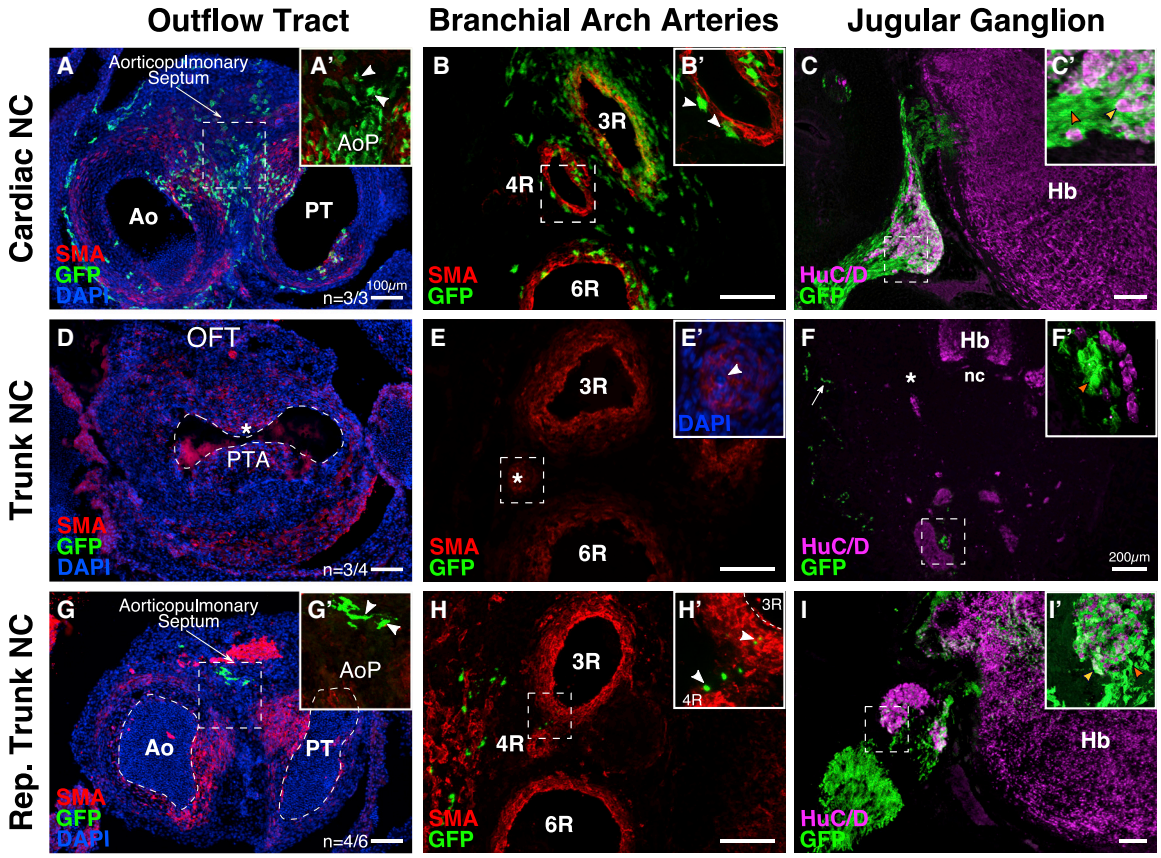

Figure 7. Reprogrammed Trunk Neural Crest Acquires Cardiac Ectomesenchymal Potential

(A–C) Sections through E6 embryos grafted with GFP$^+$ cardiac neural folds show cardiac-crest-derived cells in the aorticopulmonary septum (A, arrowheads in A′), tunica media surrounding the branchial arch arteries (B, arrowheads in B′), and neurons and satellite cells of the jugular ganglion of the vagus nerve (C and C′; orange arrowhead, satellite cells; yellow arrowhead, neurons).

(D–F) Embryos grafted with non-transfected GFP$^+$ trunk neural folds exhibit PTA (D, asterisk), abnormally constricted right-fourth branchial arch artery (E, asterisk; arrowhead in E′), and improper gangliogenesis (F, asterisk). Transplanted cells were found associated with melanocytes (arrow) and ectopic cervical nerves (F′, orange arrowheads).

(G–I) GFP$^+$ cells from the reprogrammed trunk implant migrate into the outflow tract and contribute to the aorticopulmonary septum (G, arrowheads in G′). GFP$^+$ cells were found surrounding the vessels (H, arrowheads in H′) and in neurons and satellite cells of the jugular ganglion (I and I′; orange arrowhead, satellite cells; yellow arrowhead, neurons). Ao-aorta, PT-pulmonary trunk, AoP-aorticopulmonary septum, OFT, outflow tract; Hb, hindbrain; nc, notochord; PTA, persistent truncus arteriosus.

We also noticed defects in remodeling of the pharyngeal arch arteries (Hiruma et al., 2002), as demonstrated by an abnormally constricted fourth arch artery (Figures 7E and 7E′) and lack of proper gangliogenesis (Figure 7F) in the hindbrain. To confirm that the phenotypes we observed were not artifacts of improper graft incorporation, we looked for known derivatives of resident trunk neural crest cells in the chimeras. As expected, some GFP$^+$ melanocytes (Serbedzija et al., 1994) were identified (white arrow, Figure 7F), suggesting that trunk crest cells retained their developmental potential to contribute to melanocyte precursors. Surprisingly, we found ectopic cervical nerves in proximity to the trachea in these chimeras, with GFP$^+$ satellite cells surrounding the ganglionic neurons (Figure 7F′). Taken together, these results confirmed that trunk neural crest was unable to rescue the loss of cardiac crest cells (Kirby, 1989).

However, when we grafted trunk neural fold that was "reprogrammed" by ectopic expression of *Sox8, Tgif1*, and *Ets1*, the chimeras exhibited proper septation of the outflow tract (Figures 7G and 7G″; n = 4/6), with GFP$^+$ cells present in the aorticopulmonary septum. Moreover, these embryos showed signs of proper remodeling of the pharyngeal arch arteries, as demonstrated by the presence of unconstricted arteries III, IV, and VI leading to the outflow tract, as well as a developed jugular ganglion of the vagus nerve. We found reprogrammed cells in the tunica media of these vessels (Figures 7H and 7H′), and neurons and glia of the jugular ganglia (Figures 7I and 7I′). Taken together, our results show that expression of a transcriptional program comprised of *Tgif1*, *Ets1*, and *Sox8* can confer cardiac ectomesenchymal differentiation potential onto trunk neural crest cells, essentially altering their developmental potential such that they are interchangeable with the cardiac crest.

DISCUSSION

The neural crest is a versatile cell population with great promise in regenerative medicine owing to its ability to form diverse

progeny ranging from neurons to facial cartilage and portions of the heart (Gandhi and Bronner, 2018). However, different neural crest subpopulations with distinct developmental potential exist along the body axis. Over 30 years ago, Kirby et al. (Kirby et al., 1985) defined the "cardiac neural crest" based on quail-chick chimeras as the region arising from the caudal hindbrain with the potential to form ectomesenchymal derivatives of the heart. The heart of amniotes is divided into separate systemic and pulmonary circulations such that deoxygenated blood flows from the heart to the lungs and oxygenated blood returns to the heart to be pumped through the rest of the body. The cardiac crest is critical in separating the aortic and pulmonary arteries by dividing the outflow tract via formation of the aorticopulmonary septum. Importantly, ablation of this cell population in chick embryos resulted in developmental defects of the outflow tract highly reminiscent of the human congenital birth defect PTA (Hutson and Kirby, 2003), highlighting the critical role of the cardiac crest. The cardiac crest is unique among neural crest subpopulations, since those from other axial levels are unable to rescue cardiac neural fold ablation (Kirby, 1989). In this study, we revisit these classical studies from a modern genomics perspective to identify molecular mechanisms that define the ectomesenchymal differentiation potential of the cardiac neural crest.

Our results suggest that there is left-right asymmetry with respect to contributions of the cardiac crest to the heart. While both left and right cardiac crest ablations resulted in heart defects, they differed in type and severity. Whereas removal of the left neural fold predominantly caused DORV defects (n = 6/8), ablation of the right side caused PTA (n = 4/9) and DORV (n = 3/9). These differences likely reflect left-right asymmetry in the heart itself, which undergoes dextral looping. Crest ablation also affects heart tube looping and elongation, as ablated hearts appeared bulbous with shortened and straighter outflow tract compared with controls. Remodeling of aortic arches is also asymmetric (Snider et al., 2007; Waldo et al., 1998), with selective regression of the left fourth artery in birds and unequal contribution of the left-right cardiac crest to the vagus nerve's heart innervation (Verberne et al., 2000).

Our results uncover a transcriptional program necessary for normal cardiac crest development that is sufficient to reprogram trunk neural crest cells to take on a cardiac-crest-like fate. We identify *Tgif1* as a critical factor for normal development of the cardiac crest. *Tgif1* encodes a transcriptional repressor that limits TGFβ signaling by interacting with SMADs and/or binding directly to DNA and also regulates processes like proliferation, specification, and differentiation (Bartholin et al., 2008; Hamid and Brandt, 2009). In cancer, *Tgif1* promotes the migration and growth of non-small cell lung cancer cells (Xiang et al., 2015), consistent with our findings where loss of *Tgif1* in chick caused impaired cardiac neural crest migration and reduced activity of several cardiac-crest-specific genes.

While *Tgif1* mutant mice have severe holoprosencephaly (Taniguchi et al., 2012), no apparent heart defects have been reported, possibly due to the presence of its functionally redundant paralog *Tgif2* in the murine heart (Imoto et al., 2000; Jin et al., 2005). However, *Tgif2* was not differentially enriched in migrating chick cardiac crest. The finding that *Tgif1* is important for proper outflow tract septation expands its proposed role from the central nervous system to cardiovascular development. In sea urchin embryos, *tgif* has been associated with epithelial to mesenchymal transition (EMT) (Saunders and McClay, 2014), an important process in neural crest development. However, in the cardiac crest, *Tgif1* appears to function in specification rather than EMT.

Our data show that *Sox8* functions upstream of *Tgif1*, which in turn regulates activity of *Ets1* in the migratory cardiac neural crest. We postulated that these three factors work together in a cardiac-crest-specific regulatory subcircuit. To test this, we "reprogrammed" trunk neural crest by ectopically expressing subcircuit genes and found that this is sufficient to alter their character to behave in a cardiac-crest-like manner. Transcriptional profiling of "reprogrammed" trunk neural crest cells confirmed that they became more cardiac-crest-like. Furthermore, grafting reprogrammed trunk in place of the cardiac neural folds changed their migratory and differentiative behavior such that they not only migrated into the heart but also restored septation of the outflow tract. Thus, these data show that the combination of these three factors was sufficient to imbue the transfected cells with cardiac-crest-like identity.

Of note, a relatively small number of reprogrammed trunk neural crest cells in the outflow tract appear sufficient for its septation. As crest-derived cells are relatively short lived in the outflow tract, undergoing apoptosis at later stages, one possibility is that an early interaction between cardiac crest cells and neighboring cells, likely derived from the second heart field, is sufficient for proper septation without the need for a large neural crest contribution to the septum itself. On the other hand, perhaps only small numbers of neural crest cells are required as is true in other contexts; e.g., Barlow et al. (2008) showed that a small number of enteric neural crest is sufficient to populate the entire digestive tract. In mice, reprogramming a small contingent of smooth muscle cells into melanocytes results in patent ductus arteriosus (Yajima et al., 2013).

The cardiac neural crest is specified just prior to emigration from the hindbrain. Our findings raise the intriguing possibility that these cells may be biased very early toward contributing to cardiovascular structures. Expression of genes, such as *Acta2*, *Prrx1*, and *Twist1* in a single cardiac crest cluster suggests these cells may have already acquired ectomesenchymal characteristics, as these genes are associated with the cardiac crest's ability to form the smooth muscle lining of the pulmonary arteries and the outflow tract septum. Thus, cardiac neural crest cells may acquire an ectomesenchymal identity well before they migrate into the branchial arches. Given that cells from the trunk neural crest graft delaminated from the neural tube but failed to migrate any further, it is likely that the transcriptional state of cardiac crest cells governs their ability to migrate into the corresponding branchial arches.

Together with a previously described cranial-crest-specific subcircuit important for the formation of craniofacial cartilage (Simoes-Costa and Bronner, 2016), our results suggest that small transcriptional changes can alter neural crest identity and resultant differentiative behavior along the body axis. It is interesting to note that two of the three transcription factors (*Sox8* and *Ets1*) are shared between the cardiac and cranial crest subcircuits, though *Tgif1* is unique to the cardiac region. Moreover, mutation of the Tgif1-binding site in the *Ets1* enhancer had

drastic effects on the activity of the enhancer in the cardiac but not cranial crest. This suggests that a small shift in regulatory subcircuits can have profound effects in conferring axial level identity, since grafting of the cranial neural folds in place of cardiac neural folds also resulted in PTA (Kirby, 1989). Our results not only validate the reproducibility of experiments done by Kirby and colleagues over 30 years ago (Besson et al., 1986; Kirby and Stewart, 1983; Kirby and Waldo, 1995; Kirby et al., 1985; Nishibatake et al., 1987; Phillips et al., 1987; Waldo and Kirby, 1993) but also shed light on the underlying molecular mechanisms that distinguish the cardiac neural crest from other axial levels. We posit that identification of axial level specific transcription factors and subcircuits holds the promise of identifying potentially important genes involved in proper formation of the cardiovascular system and may provide targets for identification of human genetic mutations in coding or regulatory regions. Moreover, elucidation of the gene regulatory subcircuits that underlie axial level identity will be useful for producing the full range of neural crest derivatives for the purposes of regenerative medicine.

STAR★METHODS

Detailed methods are provided in the online version of this paper and include the following:

- KEY RESOURCES TABLE
- LEAD CONTACT AND MATERIALS AVAILABILITY
- EXPERIMENTAL MODEL AND SUBJECT DETAILS
- METHOD DETAILS
  - Cardiac Neural Crest Ablation
  - Embryo Electroporation
  - Cell Sorting and Library Preparation
  - Molecular Cloning and *In Situ* Hybridization
  - Hybridization Chain Reaction
  - CRISPR-Cas9-Mediated Knockouts
  - Reprogramming Resident Trunk and Cranial Neural Crest Cells
  - Grafting Experiments
  - Sectioning and Histology
- QUANTIFICATION AND STATISTICAL ANALYSIS
  - Differential Gene Expression Analysis for Bulk RNA-seq Data
  - Bioinformatics Analysis for SMART-Seq Data
- DATA AND CODE AVAILABILITY

SUPPLEMENTAL INFORMATION

Supplemental Information can be found online at https://doi.org/10.1016/j.devcel.2020.04.005.

ACKNOWLEDGMENTS

We thank Drs. Tatjana Sauka-Spengler and Megan Martik for helpful discussions. For technical assistance, we thank Jamie Tijerina and Rochelle Diamond with the Beckman Institute (BI) Flow Cytometry Facility, Igor Antoshechkin with the Jacobs Genetics and Genomics Laboratory, Giada Spigolon and Andres Collazo with the BI Biological Imaging Facility, and Fan Gao with the BI Bioinformatics Resource Center. We thank Neil Ashley and Ivan Candido Ferreira at the Weatherall Institute (University of Oxford) for help with scRNA-seq library preparation and sequencing. This work was supported by NIH grants R01DE027568 and R01HL14058 to M.E.B. and AHA predoctoral fellowship 18PRE34050063 and Company of Biologists traveling fellowship DEVTF18119 to S.G.

AUTHOR CONTRIBUTIONS

Conceptualization, S.G. and M.E.B.; Methodology, S.G. and M.E.; Software, S.G.; Validation, S.G; Formal Analysis, S.G.; Investigation, S.G. and M.E.; Writing – Original Draft, S.G., M.E., and M.E.B.; Writing – Review & Editing, S.G. and M.E.B.; Visualization, S.G.; Supervision, M.E.B.; Funding Acquisition, M.E.B.

DECLARATION OF INTERESTS

The authors declare no competing interests.

Received: October 2, 2019
Revised: February 7, 2020
Accepted: April 6, 2020
Published: May 4, 2020

REFERENCES

Acloque, H., Wilkinson, D.G., and Nieto, M.A. (2008). In situ hybridization analysis of chick embryos in whole-mount and tissue sections. Methods Cell Biol. *87*, 169–185.

Alexa, A., and Rahnenführer, J. (2019). topGO: enrichment analysis for gene ontology. R package version 2.38.1. https://doi.org/10.18129/B9.bioc.topGO.

Anders, S., Pyl, P.T., and Huber, W. (2015). HTSeq–a python framework to work with high-throughput sequencing data. Bioinformatics *31*, 166–169.

Andrews, S.; Babraham Bioinformatics (2010). FastQC: a quality control tool for high throughput sequence data. Manual.

Arima, Y., Miyagawa-Tomita, S., Maeda, K., Asai, R., Seya, D., Minoux, M., Rijli, F.M., Nishiyama, K., Kim, K.S., Uchijima, Y., et al. (2012). Preotic neural crest cells contribute to coronary artery smooth muscle involving endothelin signalling. Nat. Commun. *3*, 1267.

Barembaum, M., and Bronner, M.E. (2013). Identification and dissection of a key enhancer mediating cranial neural crest specific expression of transcription factor, Ets-1. Dev. Biol. *382*, 567–575.

Barlow, A.J., Wallace, A.S., Thapar, N., and Burns, A.J. (2008). Critical numbers of neural crest cells are required in the pathways from the neural tube to the foregut to ensure complete enteric nervous system formation. Development *135*, 1681–1691.

Bartholin, L., Melhuish, T.A., Powers, S.E., Goddard-Léon, S., Treilleux, I., Sutherland, A.E., and Wotton, D. (2008). Maternal tgif is required for vascularization of the embryonic placenta. Dev. Biol. *319*, 285–297.

Basch, M.L., Bronner-Fraser, M., and García-Castro, M.I. (2006). Specification of the neural crest occurs during gastrulation and requires Pax7. Nature *441*, 218–222.

Bergwerff, M., Verberne, M.E., DeRuiter, M.C., Poelmann, R.E., and Gittenberger-de Groot, A.C. (1998). Neural crest cell contribution to the developing circulatory system: implications for vascular morphology? Circ. Res. *82*, 221–231.

Besson, W.T., Kirby, M.L., Van Mierop, L.H.S., and Teabeaut, J.R. (1986). Effects of the size of lesions of the cardiac neural crest at various embryonic ages on incidence and type of cardiac defects. Circulation *73*, 360–364.

Betancur, P., Bronner-Fraser, M., and Sauka-Spengler, T. (2010). Genomic code for Sox10 activation reveals a key regulatory enhancer for cranial neural crest. Proc. Natl. Acad. Sci. USA *107*, 3570–3575.

Bockman, D.E., Redmond, M.E., Waldo, K., Davis, H., and Kirby, M.L. (1987). Effect of neural crest ablation on development of the heart and arch arteries in the chick. Am. J. Anat. *180*, 332–341.

Butler, A., Hoffman, P., Smibert, P., Papalexi, E., and Satija, R. (2018). Integrating single-cell transcriptomic data across different conditions, technologies, and species. Nat. Biotechnol. *36*, 411–420.

Choi, H.M.T., Schwarzkopf, M., Fornace, M.E., Acharya, A., Artavanis, G., Stegmaier, J., Cunha, A., and Pierce, N.A. (2018). Third-generation in situ hybridization chain reaction: multiplexed, quantitative, sensitive, versatile, robust. Developement *145*, dev165753.

Dobin, A., Davis, C.A., Schlesinger, F., Drenkow, J., Zaleski, C., Jha, S., Batut, P., Chaisson, M., and Gingeras, T.R. (2013). STAR: ultrafast universal RNA-seq aligner. Bioinformatics *29*, 15–21.

Ezin, A.M., Fraser, S.E., and Bronner-Fraser, M. (2009). Fate map and morphogenesis of presumptive neural crest and dorsal neural tube. Dev. Biol. *330*, 221–236.

Franz, T. (1989). Persistent truncus arteriosus in the Splotch mutant mouse. Anat. Embryol. *180*, 457–464.

Gandhi, S., and Bronner, M.E. (2018). Insights into neural crest development from studies of avian embryos. Int. J. Dev. Biol. *62*, 183–194.

Gandhi, S., Piacentino, M.L., Vieceli, F.M., and Bronner, M.E. (2017). Optimization of CRISPR/Cas9 genome editing for loss-of-function in the early chick embryo. Dev. Biol. *432*, 86–97.

Gao, Z., Kim, G.H., Mackinnon, A.C., Flagg, A.E., Bassett, B., Earley, J.U., and Svensson, E.C. (2010). Ets1 is required for proper migration and differentiation of the cardiac neural crest. Development *137*, 1543–1551.

Grossfeld, P.D., Mattina, T., Lai, Z., Favier, R., Jones, K.L., Cotter, F., and Jones, C. (2004). The 11q terminal deletion disorder: a prospective study of 110 cases. Am. J. Med. Genet. A *129A*, 51–61.

Hamburger, V., and Hamilton, H.L. (1951). A series of normal stages in the development of the chick embryo. J. Morphol. *88*, 49–92.

Hamid, R., and Brandt, S.J. (2009). Transforming growth-interacting factor (TGIF) regulates proliferation and differentiation of human myeloid leukemia cells. Mol. Oncol. *3*, 451–463.

Harrison, T.A., Stadt, H.A., Kumiski, D., and Kirby, M.L. (1995). Compensatory responses and development of the nodose ganglion following ablation of placodal precursors in the embryonic chick (Gallus domesticus). Cell Tissue Res. *281*, 379–385.

Hiruma, T., Nakajima, Y., and Nakamura, H. (2002). Development of pharyngeal arch arteries in early mouse embryo. J. Anat. *201*, 15–29.

Hutson, M.R., and Kirby, M.L. (2003). Neural crest and cardiovascular development: a 20-year perspective. Birth Defects Res. C Embryo Today *69*, 2–13.

Imoto, I., Pimkhaokham, A., Watanabe, T., Saito-Ohara, F., Soeda, E., and Inazawa, J. (2000). Amplification and overexpression of TGIF2, a novel homeobox gene of the TALE superclass, in ovarian cancer cell lines. Biochem. Biophys. Res. Commun. *276*, 264–270.

Jin, L., Zhou, Y., Kuang, C., Lin, L., and Chen, Y. (2005). Expression pattern of TG-interacting factor 2 during mouse development. Gene Expr. Patterns *5*, 457–462.

Karolchik, D., Baertsch, R., Diekhans, M., Furey, T.S., Hinrichs, A., Lu, Y.T., Roskin, K.M., Schwartz, M., Sugnet, C.W., Thomas, D.J., et al. (2003). The UCSC genome browser database. Nucleic Acids Res. *31*, 51–54.

Kirby, M.L. (1989). Plasticity and predetermination of mesencephalic and trunk neural crest transplanted into the region of the cardiac neural crest. Dev. Biol. *134*, 402–412.

Kirby, M.L., and Stewart, D.E. (1983). Neural crest origin of cardiac ganglion cells in the chick embryo: identification and extirpation. Dev. Biol. *97*, 433–443.

Kirby, M.L., Turnage, K.L., and Hays, B.M. (1985). Characterization of conotruncal malformations following ablation of "cardiac" neural crest. Anat. Rec. *213*, 87–93.

Kirby, M.L., and Waldo, K.L. (1990). Role of neural crest in congenital heart disease. Circulation *82*, 332–340.

Kirby, M.L., and Waldo, K.L. (1995). Neural crest and cardiovascular patterning. Circ. Res. *77*, 211–215.

Kuratani, S.C., Miyagawa-Tomita, S., and Kirby, M.L. (1991). Development of cranial nerves in the chick embryo with special reference to the alterations of cardiac branches after ablation of the cardiac neural crest. Anat. Embryol. *183*, 501–514.

Kurihara, H., Kurihara, Y., Nagai, R., and Yazaki, Y. (1999). Endothelin and neural crest development. Cell. Mol. Biol. (Noisy-le-grand) *45*, 639–651.

Labun, K., Montague, T.G., Krause, M., Torres Cleuren, Y.N., Tjeldnes, H., and Valen, E. (2019). CHOPCHOP v3: expanding the CRISPR web toolbox beyond genome editing. Nucleic Acids Res. *47*, W171–W174.

Langmead, B., and Salzberg, S.L. (2012). Fast gapped-read alignment with Bowtie 2. Nat. Methods *9*, 357–359.

Loffredo, C.A. (2000). Epidemiology of cardiovascular malformations: prevalence and risk factors. Am. J. Med. Genet. *97*, 319–325.

Love, M.I., Huber, W., and Anders, S. (2014). Moderated estimation of fold change and dispersion for RNA-seq data with DESeq2. Genome Biol *15*, 550.

Martik, M.L., Gandhi, S., Uy, B.R., Gillis, J.A., Green, S.A., Simoes-Costa, M., and Bronner, M.E. (2019). Evolution of the new head by gradual acquisition of neural crest regulatory circuits. Nature *574*, 675–678.

Martin, M. (2011). Cutadapt removes adapter sequences from high-throughput sequencing reads. EMBnet.journal *17*, 10–12.

McGrew, M.J., Sherman, A., Lillico, S.G., Ellard, F.M., Radcliffe, P.A., Gilhooley, H.J., Mitrophanous, K.A., Cambray, N., Wilson, V., and Sang, H. (2008). Localised axial progenitor cell populations in the avian tail bud are not committed to a posterior Hox identity. Development *135*, 2289–2299.

Miyagawa-Tomita, S., Waldo, K., Tomita, H., and Kirby, M.L. (1991). Temporospatial study of the migration and distribution of cardiac neural crest in quail-chick chimeras. Am. J. Anat. *192*, 79–88.

Narayanan, C.H., and Narayanan, Y. (1980). Neural crest and placodal contributions in the development of the glossopharyngeal-vagal complex in the chick. Anat. Rec. *196*, 71–82.

Neeb, Z., Lajiness, J.D., Bolanis, E., and Conway, S.J. (2013). Cardiac outflow tract anomalies. Wiley Interdiscip. Rev. Dev. Biol. *2*, 499–530.

Nishibatake, M., Kirby, M.L., and Van Mierop, L.H.S. (1987). Pathogenesis of persistent truncus arteriosus and dextroposed aorta in the chick embryo after neural crest ablation. Circulation *75*, 255–264.

O'Donnell, M., Hong, C.S., Huang, X., Delnicki, R.J., and Saint-Jeannet, J.P. (2006). Functional analysis of Sox8 during neural crest development in Xenopus. Development *133*, 3817–3826.

Phillips, M.T., Kirby, M.L., and Forbes, G. (1987). Analysis of cranial neural crest distribution in the developing heart using quail-chick chimeras. Circ. Res. *60*, 27–30.

Picelli, S., Faridani, O.R., Björklund, A.K., Winberg, G., Sagasser, S., and Sandberg, R. (2014). Full-length RNA-seq from single cells using Smart-seq2. Nat. Protoc. *9*, 171–181.

Sauka-Spengler, T., and Barembaum, M. (2008). Gain- and loss-of-function approaches in the chick embryo. Methods Cell Biol. *87*, 237–256.

Saunders, L.R., and McClay, D.R. (2014). Sub-circuits of a gene regulatory network control a developmental epithelial-mesenchymal transition. Development *141*, 1503–1513.

Schindelin, J., Arganda-Carreras, I., Frise, E., Kaynig, V., Longair, M., Pietzsch, T., Preibisch, S., Rueden, C., Saalfeld, S., Schmid, B., et al. (2012). Fiji: an open-source platform for biological-image analysis. Nat. Methods *9*, 676–682.

Serbedzija, G.N., Bronner-Fraser, M., and Fraser, S.E. (1994). Developmental potential of trunk neural crest cells in the mouse. Development *120*, 1709–1718.

Simoes-Costa, M., and Bronner, M.E. (2016). Reprogramming of avian neural crest axial identity and cell fate. Science *352*, 1570–1573.

Simões-Costa, M.S., McKeown, S.J., Tan-Cabugao, J., Sauka-Spengler, T., and Bronner, M.E. (2012). Dynamic and differential regulation of stem cell factor FoxD3 in the neural crest is encrypted in the genome. PLoS Genet. *8*, e1003142.

Snider, P., Olaopa, M., Firulli, A.B., and Conway, S.J. (2007). Cardiovascular development and the colonizing cardiac neural crest lineage. ScientificWorldJournal *7*, 1090–1113.

Taniguchi, K., Anderson, A.E., Sutherland, A.E., and Wotton, D. (2012). Loss of tgif function causes holoprosencephaly by disrupting the Shh signaling pathway. PLoS Genet. *8*, e1002524.

Tani-Matsuhana, S., Vieceli, F.M., Gandhi, S., Inoue, K., and Bronner, M.E. (2018). Transcriptome profiling of the cardiac neural crest reveals a critical role for MafB. Dev. Biol. *444*, S209–S218.

Trapnell, C., Cacchiarelli, D., Grimsby, J., Pokharel, P., Li, S., Morse, M., Lennon, N.J., Livak, K.J., Mikkelsen, T.S., and Rinn, J.L. (2014). The dynamics and regulators of cell fate decisions are revealed by pseudotemporal ordering of single cells. Nat. Biotechnol. *32*, 381–386.

Trapnell, C., Roberts, A., Goff, L., Pertea, G., Kim, D., Kelley, D.R., Pimentel, H., Salzberg, S.L., Rinn, J.L., and Pachter, L. (2012). Differential gene and transcript expression analysis of RNA-seq experiments with TopHat and Cufflinks. Nat. Protoc. *7*, 562–578.

Verberne, M.E., Gittenberger-de Groot, A.C., Van Iperen, L., and Poelmann, R.E. (2000). Distribution of different regions of cardiac neural crest in the extrinsic and the intrinsic cardiac nervous system. Dev. Dyn. *217*, 191–204.

Waldo, K., Miyagawa-Tomita, S., Kumiski, D., and Kirby, M.L. (1998). Cardiac neural crest cells provide new insight into septation of the cardiac outflow tract: aortic sac to ventricular septal closure. Dev. Biol. *196*, 129–144.

Waldo, K.L., and Kirby, M.L. (1993). Cardiac neural crest contribution to the pulmonary artery and sixth aortic arch artery complex in chick embryos aged 6 to 18 days. Anat. Rec. *237*, 385–399.

Xiang, G., Yi, Y., Weiwei, H., and Weiming, W. (2015). TGIF1 promoted the growth and migration of cancer cells in nonsmall cell lung cancer. Tumour Biol. *36*, 9303–9310.

Yajima, I., Colombo, S., Puig, I., Champeval, D., Kumasaka, M., Belloir, E., Bonaventure, J., Mark, M., Yamamoto, H., Taketo, M.M., et al. (2013). A subpopulation of smooth muscle cells, derived from melanocyte-competent precursors, prevents patent ductus arteriosus. PLoS One *8*, e53183.

Ye, M., Coldren, C., Liang, X., Mattina, T., Goldmuntz, E., Benson, D.W., Ivy, D., Perryman, M.B., Garrett-Sinha, L.A., and Grossfeld, P. (2010). Deletion of ETS-1, a gene in the Jacobsen syndrome critical region, causes ventricular septal defects and abnormal ventricular morphology in mice. Hum. Mol. Genet. *19*, 648–656.

STAR★METHODS

KEY RESOURCES TABLE

REAGENT or RESOURCE	SOURCE	IDENTIFIER
Antibodies		
Mouse IgG1 anti-Pax7	Developmental Studies Hybridoma Bank at University of Iowa	RRID: AB_528428
Rabbit anti-Sox2	Abcam	Cat#ab97959; RRID: AB_2341193
Mouse IgG2b anti-MF20	Developmental Studies Hybridoma Bank at University of Iowa	RRID: AB_2147781
Mouse IgM anti-HNK1	Developmental Studies Hybridoma Bank at University of Iowa	RRID: AB_2314644
Mouse IgG2a anti-SMA	Sigma	Cat#3879S; RRID: AB_2255011
Mouse IgG2b anti-HuC/D	Invitrogen	Cat# A21271; RRID: AB_221448
Goat IgG anti-GFP	Rockland	Cat# 600-101-215; RRID: AB_218182
Mouse IgG2a anti-V5	Invitrogen	Cat#R960-25; RRID: AB_2556564
Rabbit anti-RFP	MBL	Cat#PM005; RRID: AB_591279
Critical Commercial Assays		
RNAqueous Micro Total RNA isolation kit	Ambion	Cat#AM1931
SmartSeq2 V4 kit	Takara Clontech	Cat#634889
Nextera XT DNA library preparation kit	Illumina	Cat#FC-131-1024
Qubit High sensitivity DNA kit	Thermo Fisher Scientific	Cat#Q32854
NEB Next High-Fidelity 2X PCR Master Mix	New England Biolabs	Cat#M0543S
NextSeq 500/550 High Output Kit v2 (75 cycles)	Illumina	Cat#FC-404-2005
Endofree maxi prep kit	Macharey Nagel	Cat#740426.50
Agencourt AMPure XP beads	Beckman Coulter	Cat#A63880
illustra MicroSpin G-50 Columns	GE Healthcare Life Sciences	Cat# 27533001
Hybridization Chain Reaction	Molecular Technologies	NA
Deposited Data		
Raw and analyzed data	This paper	BioProject ID PRJNA515142
Software and Algorithms		
Fiji/ImageJ	Schindelin et al., 2012	https://imagej.nih.gov/ij/
Bowtie2	Langmead and Salzberg, 2012	http://bowtie-bio.sourceforge.net/bowtie2/index.shtml
Samtools	N/A	http://samtools.sourceforge.net/
HTSeq-count	N/A	https://htseq.readthedocs.io/en/release_0.11.1/count.html
Seurat	Butler et al., 2018	https://satijalab.org/seurat/
Oligonucleotides		
GCAGGTGTAGTTGCAATATC	This paper	Tgif1.1.gRNA
GTTGGTCCCCCGCCGTGAGA	This paper	Tgif1.2.gRNA
GGGTCATGTTGAGCATTTGG	This paper	Sox8.1.gRNA
gTCCACCTTAGCGCCCAGCG	This paper	Sox8.2.gRNA
GACGCGACGCCCATCCTCAA	This paper	Sox8.3.gRNA
GGCCTCAACCATGAAGGCGG	This paper	Ets1.1.gRNA
GACCTTCAGTGGCTTCGCAA	This paper	Ets1.2.gRNA
GAGAGACGCACGTGCGGGAC	This paper	Ets1.3.gRNA
GAAAGTCAGGCGCTAGCTCC	This paper	Ets1.4.gRNA

LEAD CONTACT AND MATERIALS AVAILABILITY

Further information and requests for resources and reagents should be directed to the Lead Contact, Marianne Bronner (mbronner@caltech.edu). All plasmids (enhancers, expression constructs, and CRISPR) and protocols used in this study will be made available upon request.

EXPERIMENTAL MODEL AND SUBJECT DETAILS

Fertilized chicken eggs were purchased from Sun State Valley farm (CA) and incubated at 37°C for 33-36h to get HH9+ embryos for ablation and reprogramming experiments. Transgenic eggs were obtained from Clemson University through Dr. Susan Chapman. All experiments were performed on chick embryos younger than E10 and were therefore not subjected to IACUC regulations.

METHOD DETAILS

Cardiac Neural Crest Ablation

Windows were made in the eggs and 2% blue food dye solution was injected under the embryo to provide contrast. Unilateral and bilateral ablations were performed using glass needles by surgically removing the dorsal neural tube at the level of the mid-otic vesicle to the caudal edge of somite 3 as previously described (Kirby, 1989). The embryos were sealed with surgical tape and incubated at 37°C *in ovo* for 3 or 6-6.5 days.

Embryo Electroporation

Ex ovo electroporations were performed as previously described (Sauka-Spengler and Barembaum, 2008) by passing 5 electric pulses every 50ms at an interval of 100ms at 5.2V. The electroporated embryos were cultured in sterile petridishes in 1mL albumin supplemented with penicillin/streptomycin at 37°C until HH9+ or HH12. *pCAG>H2B-RFP* was electroporated as a marker for transfection efficiency and was used to discard embryos with poor transfection. For *in ovo* electroporations, fertilized eggs were incubated for 33-36h to get HH9 embryos. The DNA solution was injected into the lumen of the neural tube and the right side transfected by passing 5 electric pulses every 30ms at an interval of 100ms at 18V. The egg shell was sealed with surgical tape and the eggs were incubated at 37°C until they reached the desired stage. Fluorescence was checked under a Leica epifluorescence scope and embryos with improper morphology and/or poor transfection were discarded.

Cell Sorting and Library Preparation

To sort cardiac and trunk neural crest cells, HH4 and HH9 embryos were electroporated with FoxD3-NC2>mCherry (Simões-Costa et al., 2012) *ex ovo* and *in ovo*, respectively. To sort reprogrammed trunk neural crest cells, HH9 embryos were electroporated with expression constructs for *Sox8*, *Tgif1*, and *Ets1* along with Sox10E2>GFP. The embryos were cultured until HH12 to isolate cardiac neural crest and HH18 to isolate wild-type and reprogrammed trunk neural crest. The embryos were dissected between the otic vesicle and somite 3 and between somite 18 and 25 for cardiac and trunk neural crest, respectively. For cell dissociation, the dissected tissue was collected in chilled 1X DPBS, washed thrice, and incubated in Accumax cell dissociation solution (EMD Millipore) for 15 minutes at 37°C, with gentle pipetting every 5 minutes. Once the tissue appeared dissociated, Hanks Buffered Saline Solution (HBSS) (Corning) supplemented with 25mM HEPES (pH 7), BSA Fraction V (Sigma; 0.2% w/v), and 10mM $MgCl_2$ was used to terminate dissociation. Cells were collected at the bottom by spinning the solution at 300g for 4 minutes and resuspended in 1mL HANKS-$MgCl_2$. The cells were then passed through a 40μm filter to remove debris and undissociated clumps. $mCherry^+$ cells were sorted on a Sony Synergy 3200 cell sorter equipped with a 561 nm laser at the Caltech Flow Cytometry Facility. Sytox Blue staining was used to label dead cells during the sorting run.

For bulk RNA-seq, the SMART-Seq v4 Ultra Low Input RNA Kit for sequencing was used by following the manufacturer's protocol (Takara Bio). Briefly, the sorted cells were washed thrice in chilled sterile 1x PBS. cDNA was synthesized using the 3' SMART-Seq CDS Primer II A (followed by template switching with the SMART-Seq v4 Oligonucleotide primer) and amplified using the following program: 95°C for 1 min, 15 cycles of 98°C for 10s, 65°C for 30s, and 68°C for 3min, and a final extension at 72°C for 10min. The amplified cDNA was purified using AMPure beads (Agencourt) and the quality was confirmed on the Agilent 2100 Bioanalyzer using a high sensitivity DNA chip. The library was prepared by Igor Antoshechkin at the Caltech Genomics Facility and sequenced on a HiSeq 2500 to obtain 50 million single end reads.

For scRNA-seq, individual neural crest cells were collected in 96-well plates by FACS at the MRC Weatherall Institute of Molecular Medicine at the University of Oxford. Sequencing libraries were prepared as previously described (Picelli et al., 2014). Libraries were sequenced on the Illumina NextSeq500 platform using single end 75bp sequencing chemistry.

Molecular Cloning and *In Situ* Hybridization

Overexpression constructs for *Ets1* and *Sox8* were generously provided by Marcos Simões-Costa and Meyer Barembaum, respectively. The coding sequence for *Tgif1* was obtained from the UCSC genome browser (Karolchik et al., 2003) and amplified using Accuprime polymerase (ThermoFisher). A V5 epitope tag was fused to the N-terminus to allow for construct validation using immuno-

histochemistry. This fusion gene was then cloned under the regulation of the CAGG promoter. Tgif1 and Ets1 enhancers were amplified from genomic DNA using Accuprime polymerase (ThermoFisher).

RNA was extracted from HH12 embryos using an optimized TRIzol-chloroform extraction protocol. SuperScript III Reverse Transcriptase was used to synthesize cDNA using oligo dT primers and PCR program recommended by the manufacturer. Cardiac crest genes were amplified from this cDNA and cloned in *pBluescript* plasmid. All RNA probes were synthesized using Digoxigenin-labeled UTPs and diluted in Hybridization buffer containing 50% formamide, 5mM EDTA, 1.3x SSC, 200μg/mL tRNA, 0.2% Tween-20, 0.5% CHAPS, and 100μg/mL heparin. All probes were used at a final concentration ranging between 2-5ng/μL. *In situ* hybridization was performed using a previously described protocol (Acloque et al., 2008).

Hybridization Chain Reaction

HCR v3 was performed using the protocol suggested by Molecular Technologies (Choi et al., 2018). Briefly, the embryos were cultured to desired stages and fixed in 4% paraformaldehyde overnight at 4°C. On day 2, the fixed embryos were washed in 0.1% PBS-Tween and dehydrated using a series of 25%, 50%, 75%, and 100% methanol. Following an overnight incubation at -20°C in 100% methanol, the embryos were rehydrated, treated with proteinase-K for 2.5 minutes, and incubated with 5-10pmol of probe mixture overnight at 37°C. On day 3, excess probe was washed off and the embryos were incubated with 30pmol of both hairpins H1 and H2 at room temperature overnight. On day 4, the embryos were washed in 0.1% 5x-SSC-Tween and imaged on a Zeiss Imager M2 with an ApoTome module and/or Zeiss LSM 880 confocal microscope at the Caltech Biological Imaging Facility.

CRISPR-Cas9-Mediated Knockouts

The genomic loci for Tgif1, Sox8, and Ets1 were obtained from the UCSC genome browser (Karolchik et al., 2003). Two gRNA targets were generated to knock out Tgif1: Tgif1.1 (5'- GCAGGTGTAGTTGCAATATC -3') and Tgif1.2 (5'- GTTGGTCCCCCGCCGTGAGA -3'), three gRNA targets were generated to knock out Sox8: Sox8.1 (5' – GGGTCATGTTGAGCATTTGG -3'), Sox8.2 (5'- gTCCACCTTAGCGCCCAGCG -3'), and Sox8.3 (5'- GACGCGACGCCCATCCTCAA -3'), and four gRNA targets were generated to knock out Ets1: Ets1.1 (5'- GGCCTCAACCATGAAGGCGG -3'), Ets1.2 (5'- GACCTTCAGTGGCTTCGCAA -3'), Ets1.3 (5'- GAGAGACGCACGTGCGGGAC -3'), and Ets1.4 (5'- GAAAGTCAGGCGCTAGCTCC -3') using CHOPCHOP (Labun et al., 2019). The protospacers were cloned in a modified f+e gRNA backbone downstream of the chick U6.3 promoter. For contralateral control electroporations, we used the control gRNA described in (Gandhi et al., 2017). Gastrula HH4 embryos were bilaterally electroporated with *CAGG>nls-Cas9-nls* (2 μg/μl) and *CAGG>H2B-RFP* (2 μg/μl) together with either Tgif1 gRNAs (0.75 μg/μl each), or Sox8 gRNAs (0.5μg/μl each), or Ets1 gRNAs (0.375μg/μl each) on the right side and *U6.3>control.gRNAf+e* (1.5 μg/μl) on the left side. The embryos were then cultured *ex ovo* until HH12, assayed for good transfection efficiency and morphology, and processed for whole mount *in situ* hybridization and HCR.

Reprogramming Resident Trunk and Cranial Neural Crest Cells

Enhancer element governing the expression of Sox10 (E2) (Betancur et al., 2010) was cloned under the regulation of a constitutive HSV thymidine kinase promoter driving GFP expression. To test whether *Tgif1* alone can reprogram trunk neural crest cells, HH9+ embryos were unilaterally co-electroporated with overexpression constructs *CAGG>V5-Tgif1* (2.5μg/μl each) and the enhancer construct *pTK-Sox10E2>GFP* (2μg/μl) *in ovo* as described above. The eggs were sealed and incubated at 37°C until HH14 to look for enhancer activity. The embryos were screened for the expression of *H2B-RFP* and fixed for antibody staining against GFP. To test the effect of reprogramming on resident trunk neural crest cells, HH9+ embryos were electroporated with *CAGG>V5-Tgif1*, *CAGG>Ets1*, and *CAGG>Sox8-IRES-H2B-RFP* (2μg/μl each) on the right side *in ovo*. The embryos were developed to until HH18 and fixed for HCR. To test the effect of reprogramming on resident cranial neural crest cells, HH4 embryos were electroporated with the three expression constructs (2μg/μl each) on the right side. The left side was electroporated with *CAGG>H2B-RFP (2.5μg/μl)* and served as an internal control. The embryos were cultured *ex ovo* until HH9+, after which they were fixed for *in situ* hybridization.

Grafting Experiments

Wild-type chicken embryos served as hosts in our transplants and were incubated at 37°C until HH9+/HH10 (8-10 somite stage). Donor transgenic Roslin Green GFP eggs, in which CAGGS (CMV enhancer/beta actin promoter/first intron) drives eGFP expression (McGrew et al., 2008) were incubated to HH14 or to the same stage as their wild-type counterparts. Precautions taken to ensure a high survival rate post-surgery consisted of maintaining high humidity levels (80-100%) in an environment free of fungal contamination. All eggs were individually cleaned with 70% ethanol before incubation; incubators, plastic egg trays and water tanks were treated with methylene blue to avoid any fungal infection. Host embryos were prepared by removing, unilaterally, the dorsal neural tube of wild-type stage 9+/10 host embryos from the level of the mid-otic vesicle to the caudal edge of somite 3. For positive controls (cardiac to cardiac), a similar microsurgical procedure was carried out on a stage-matched donor transgenic embryo. A homochronic, homotopic graft was completed, with the transgenic dorsal neural tube used as donor tissue to replace the section of dorsal neural tube removed from the wild-type host. Negative control embryos (trunk to cardiac) were generated similarly, with the difference that the donor tissue originated from the trunk level of a stage 14 donor transgenic embryo, specifically from somite 18 to approximately somite 24. In our experimental group (reprogrammed trunk to cardiac), the reprogrammed transgenic dorsal neural

tube originated from a stage 14 transgenic donor, previously electroporated with the regulatory sub-circuit genes *Tgif1*, *Ets1,* and *Sox8* at HH9. Reprogrammed dorsal neural tube was inserted in place of the host dorsal neural tube. Post-surgery, the host eggs were sealed with surgical tape and incubated until HH18-20 (E4) and stage 31-34 (E6).

Sectioning and Histology

E4 and E6 chimeric embryos were washed in 5% (room temperature, 30min) and 15% sucrose (4°C, overnight) and incubated overnight in gelatin at 37°C. The next day, they were embedded in plastic molds, frozen in liquid nitrogen, and stored at -80°C for at least 4 hours. The embedded embryos were then sectioned on a micron cryostat to obtain 16μm sections. Immunohistochemistry on sections was performed using a previously described protocol (Ezin et al., 2009). Briefly, the sections were degelatinized at 42°C in 1x PBS for 5 minutes and blocked in PBS-0.3%Triton supplemented with 10% goat or donkey serum. The sections were incubated in primary antibodies overnight at 4°C. The next day, slides were washed thrice in 1x PBS, and the sections were incubated in secondary antibodies for 1h at room temperature. Following 2 washes in 1x PBS, the slides were soaked in 1x PBS containing 0.1μg/mL DAPI for 5 minutes. The slides were then washed once each in 1x PBS and distilled water. Transverse sections were imaged on a Zeiss Imager M2 with an ApoTome module and/or Zeiss LSM 880 confocal microscope at the Caltech Biological Imaging Facility. All post-processing was done using FIJI imaging software (Schindelin et al., 2012). Early stage embryos (HH10-12) were sectioned using the same protocol as described but with a 6h instead of overnight incubation in gelatin at 37°C.

The following primary antibodies were used: Mouse IgG1 anti-Pax7 (DSHB; 1:10), Rabbit anti-Sox2 (Abcam ab97959; 1:500), Mouse IgG2b anti-MF20 (DSHB; 1:100), Mouse IgM anti-HNK1 (DSHB; 1:5), Mouse IgG2a anti-SMA (Sigma Cat# A5228; 1:500), Mouse IgG2b anti-HuC/D (Invitrogen – Cat# A21271; 1:500), Goat anti-GFP (Rockland Cat# 600-101-215; 1:500), Mouse IgG2a anti-V5 (Invitrogen Cat# R96025; 1:200), and Rabbit anti-RFP (MBL Cat# PM005; 1:500). The signal was detected using the following secondary antibodies: Goat anti-Mouse Alexa Fluor 647 (for Pax7; 1:250), Goat anti-Mouse IgM Alexa Fluor 350 (for HNK1; 1:250), Goat anti-rabbit Alexa Fluor 488 (for Sox2; 1:500), Donkey anti-goat Alexa Fluor 488 (for GFP; 1:500), Goat anti-mouse IgG2a Alexa Fluor 568 (for SMA and V5; 1:500), Goat anti-mouse IgG2b Alexa Fluor 633 (for HuC/D and MF20: 1:250), and Goat anti-rabbit IgG1 Alexa Fluor 568 (for RFP; 1:500).

QUANTIFICATION AND STATISTICAL ANALYSIS

Differential Gene Expression Analysis for Bulk RNA-seq Data

The reads obtained from the HiSeq run were demultiplexed and filtered using custom scripts. The filtered reads were checked for quality using *fastqc* (Andrews and Babraham Bioinformatics, 2010). Based on the traces, the reads were trimmed by 10bp at the 3' end and overrepresented sequences (adapter and poly A tail) were removed using *cutadapt* (Martin, 2011). These 40bp reads were then mapped to the chicken genome (galgal6.0 assembly) obtained from Ensembl using *Bowtie2* (Langmead and Salzberg, 2012). Transcript counts were calculated using *HTseq-count* (Anders et al., 2015), and differential gene expression analysis was performed using *DESeq2* (Love et al., 2014). For our analysis, cardiac neural crest genes were directly compared with trunk neural crest genes. Genes with fold change ≥ 2 and adjusted p-value ≤ 0.05 were considered "enriched and significant" and were included in subsequent analysis. For reprogrammed trunk neural crest comparison, we generated a normalized transcript count matrix as described in (Martik et al., 2019) and plotted relative values for top genes that have previously been shown to be required for neural crest development at cardiac and trunk axial levels as a heatmap.

Bioinformatics Analysis for SMART-Seq Data

The raw fastq data of 75-bp single-end sequencing reads were aligned to the chicken galgal6 reference genome using STAR-2.7.0 software (Dobin et al., 2013). The mapped reads were further processed by Cufflinks 2.2 (Trapnell et al., 2012) using the chick gene annotation file obtained from Ensembl to estimate transcript abundance. Relative abundance of transcripts was measured by fragments per kilobase of exon per million fragments mapped (FPKM). For each library, we computed total number of sequencing reads, number of uniquely mapped reads, mapping rate and number of genes detected. We selected cells with more than 100K total reads for downstream analysis. The data was filtered, normalized, and scaled using Seurat v3 (Butler et al., 2018), and all plots were generated using the in-built functions. For GO term analysis, the Bioconductor package topGO (Alexa and Rahnenführer, 2019) was used using default parameters. Adjusted p-values were calculated using Fisher's exact test. The heatmap showing relative expression values for different genes was generated using a normalized matrix as described above. Representative genes for each population (progenitor, proliferative, ectomesenchymal, and Schwann cell-like) were selected for the heatmap. Pseudotime trajectories were generated using Monocle v2 (Trapnell et al., 2014) by following standard instructions from the authors.

DATA AND CODE AVAILABILITY

All sequencing data are available on NCBI (BioProject ID PRJNA515142). Custom scripts written for data analysis are available from the lead contact upon request.